

**Development of a FRET biosensor for ROCK based on a consensus substrate sequence identified by KISS technology**

**Chunjie Li**

## Table of Contents

<b>Abstract .....</b>	<b>2</b>
<b>Chapter 1 Introduction .....</b>	<b>3</b>
1-1 Rho-family GTPases .....	4
1-2 Rho-associated protein kinase.....	5
1-3 FRET biosensor .....	7
1-4 Kinase-interacting substrate screening .....	8
<b>Chapter 2 Experimental Procedures .....</b>	<b>10</b>
2-1 Reagents.....	11
2-2 FRET biosensors and plasmids.....	11
2-3 Cell culture and transfection.....	14
2-4 Time-lapse FRET imaging.....	16
2-5 Small interfering RNA transfection.....	17
2-6 Western blotting .....	17
<b>Chapter 3 Results and Discussion .....</b>	<b>19</b>
3-1 Design of FRET biosensor for ROCK based on KISS .....	20
3-2 Specificity and sensitivity of Eevee-ROCK.....	22
3-3 Effect of siRNA-mediated silencing of ROCK expression and RhoA mutants on the FRET ratio of Eevee-ROCK.....	26
3-4 Effect of subcellular localization on ROCK activity .....	29
3-5 ROCK activation at M phase and early G1 phase .....	31
3-6 ROCK activation during apoptosis .....	34
<b>Chapter 4 Conclusion .....</b>	<b>37</b>
<b>Bibliography.....</b>	<b>42</b>
<b>Acknowledgment .....</b>	<b>55</b>

## **Abstract**

Rho-associated protein kinase (ROCK) is a serine-threonine protein kinase, which regulates the shape and movement of cells by acting on the cytoskeleton. ROCK can phosphorylate a number of cytoskeleton-related molecules such as adducin, ezrin-radixin-moesin proteins, LIM kinase, myosin light chain (MLC) and MLC phosphatase. To study the spatio-temporal regulation of ROCK, in this study I developed a highly specific fluorescence resonance energy transfer (FRET) biosensor for ROCK, named Eevee-ROCK. The kinase-specific substrate peptide was identified by kinase-interacting substrate screening (KISS) technology, which deduces a consensus substrate sequence for the protein kinase. The efficiency of Eevee-ROCK was quantified in HeLa cells. The FRET level was increased by the known stimulator of ROCK such as epidermal growth factor (EGF), lysophosphatidic acid (LPA), and serum and decreased by ROCK inhibitors, Y27632, GSK429286 and HA1077. The treatment of siRNAs against ROCK illustrated that the basal FRET signal of Eevee-ROCK derived from the activities of both ROCK1 and ROCK2. With the stable expression of Eevee-ROCK in HeLa cells, I found ROCK was rapidly re-activated concomitant with the spreading of cells on the culture dishes after cytokinesis, consistent with previous reports about the essential roles of ROCK in cell cycle progression. Moreover, Eevee-ROCK revealed a substantial activation of ROCK during apoptosis induced by TNF- $\alpha$  and cycloheximide. Taken together, the ROCK biosensor that I developed in this study will benefit us for a better understanding of the role of ROCK in a physiological context.

# **Chapter 1**

## **Introduction**

## 1-1 Rho-family GTPases

The Rho-family proteins, a subfamily of the Ras superfamily, are defined by the presence of a Rho-type GTPase-like domain. Similar with Ras proteins, Rho-family proteins contain the sequence motifs binding to GDP and GTP with high affinity, and change between the active states and the inactive states. During the signal transduction, guanine nucleotide exchange factors (GEFs) promote the exchange of GDP to GTP, producing the active state of the proteins, and GTPase-activating proteins (GAPs) enhance the hydrolysis of the bound GTP molecules, resulting in the transfer of the GTPase back to the inactivate form (Fig. 1). The activated Rho-family proteins interact with the downstream effectors to stimulate signaling pathways that mediate the diverse function of Rho-family proteins. Rho-family proteins are known to be able to regulate cell morphology, the actin cytoskeleton, and affect gene expression, cell proliferation and survival, which are important in tumorigenesis (Valencia *et al.*, 1991; Van and D'Souza-Schorey, 1997; Hall, 1998; Wennerberg and Der, 2004).

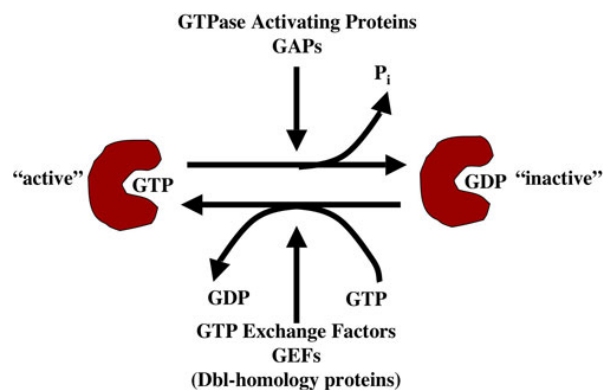


**Figure 1. Rho family GTPases function as molecular switches between GDP-bound and GTP-bound forms.** GAPs increase GTPase activity to form the inactive, GDP-bound state, while GEFs enhance the exchange of GDP with GTP to form the active, GTP-bound state.

In order to perform their biological functions, most Rho-family proteins required the docking onto cell membranes in the manner different with Ras proteins. The anchoring step requires the cooperation of intrinsic tethering signals rather than the achievement by default during the biosynthesis (Winter-Vann and Casey, 2005). The most important tethering signal is the so-called GTPase "CAAX box". With different cell lines, the localization of Rho-family proteins is quite different because of the

modulation by a complicated system of cell type-dependent regulatory pathways (Bustelo *et al.*, 2007).

Many effectors of Rho-family proteins are kinases, which phosphorylate cellular targets and control cellular functions. To date, the best-known members of Rho-family proteins are RhoA, Rac1 and CDC42, and the most characterized effector kinases are the RHO-associated coiled-coil-forming kinase (ROCK), which binds active RhoA, and the p21-activated kinases (PAKs), which bind active CDC42 and Rac1. The small GTPase RhoA is a member of Rho subgroup, which consists of RhoA, RhoB and RhoC. All of these three isoforms are highly homologous, and can lead to stress fiber formation with the overexpression in fibroblasts (Wheeler and Ridley, 2004). RhoA was also found to control cell adhesion and motility via actin-cytoskeleton reorganization and actomyosin contraction (Etienne-Manneville and Hall, 2002; Fukata *et al.*, 2003). CDC42 could associate with actin cytoskeleton, whereas Rac1 could relocate to the plasma membrane (Azim *et al.*, 2000), and the activations of CDC42 and Rac1 are thought to induce actin-rich filopodia and lamellipodia, respectively (Ridley *et al.*, 1992; Nobes and Hall, 1995). PAKs are serine/threonine kinases that serve as the downstream effectors of Rho GTPase CDC42 and Rac. They bind to Rho GTPase CDC42 and Rac through a GTPase Binding Domain (GBD). PAKs has an N-terminal regulatory domain, a proline-rich domain, and a C-terminal terminal kinase domain (Manser *et al.*, 1994; Knaus *et al.*, 1995). At least 4 isoforms of PAKs have been reported in mammals, and the activation of PAKs resulted both from the binding of Rho GTPase CDC42 and Rac, and from the autophosphorylation of serine/threonine residues in the N-terminal regulatory domain (Knaus *et al.*, 1998; Zenke *et al.*, 1999; Chong *et al.*, 2001).

## **1-2 Rho-associated protein kinase**

Rho-associated protein kinase (ROCK) was isolated as a target protein of RhoA (Leung *et al.*, 1995; Ishizaki *et al.*, 1996; Matsui *et al.*, 1996), and has been shown to play pivotal roles in actomyosin contraction and the induction of actomyosin bundles (Narumiya *et al.*, 2009). ROCK has been shown to induce actomyosin contraction via phosphorylation of MLC or the myosin-binding subunit of MLC phosphatase (Amano *et al.*, 1996; Kimura *et al.*, 1996; Uehata *et al.*, 1997).

ROCK is composed of three major domains: a kinase domain responsible for the catalytic activity at the N-terminus, a coiled-coil domain containing the Rho-binding

site and a pleckstrin homology (PH) domain including cysteine-rich domain at the C-terminus (Nakagawa *et al.*, 1996). The ROCK family contains two members, ROCK1 and ROCK2. ROCK1 is also called ROCK I, ROK $\beta$ , rho-kinase  $\beta$ , or p160ROCK, and ROCK2 is also called ROCK II, ROK $\alpha$ , or Rho kinase (Riento and Ridley, 2003). They share 65% identity in their primary amino acid sequences, and 92% identity in the kinase domain. In humans, ROCK1 is located on chromosome 18 (18q11.1), and encodes 1354 amino acids, whereas ROCK2 is located on chromosome 2 (2p24), and encodes 1388 amino acids (Pelosi *et al.*, 2007). The distribution of ROCK1 and ROCK2 is almost similar in the different tissues (Julian and Olson, 2014). There are some few specific tissues with dramatically higher expression levels of one isoform than the other. For example, in the tissues like thymus and blood, ROCK1 is predominant, whereas in the brain and heart, ROCK2 is preferentially found (Schmandke *et al.*, 2007; Julian and Olson, 2014). The subcellular localization of both ROCK1 and ROCK2 has been well characterized. Several reports present a predominantly cytoplasmic expression of ROCK1 in cells, and the association of ROCK1 with the plasma membrane and centrosomes (Glyn *et al.*, 2003; Stroeken *et al.*, 2006; Chevrier *et al.*, 2002). Some studies also reported a predominantly cytosolic distribution of ROCK2, and the overexpression of RhoA lead to the recruitment of ROCK2 to internal and peripheral cell membranes, associating with actin microfilaments (Leung *et al.*, 1995; Matsui *et al.*, 1996; Vandenabeele *et al.*, 2010). Other studies reported the accumulation of ROCK2 at the cleavage furrow, consistent with the role of ROCK in the formation of contractile ring during cytokinesis (Kosako *et al.*, 1999; Inada *et al.*, 1999). Further studies also revealed that in serum-starved cells, ROCK2 was distributed in stress fibers, filamentous vimentin network, the centrosomes, and the nucleus of growing cells (Tanaka *et al.*, 2006; Katoh *et al.*, 2001; Kawabata *et al.*, 2004; Sin *et al.*, 1998; Ma *et al.*, 2006).

ROCK1 and ROCK2 can be regulated in Rho-dependent and Rho-independent manners. In the inactive state, the C-terminal of ROCK behaves as an auto-inhibitory region. When the Rho binding domain (RBD) of ROCK binds to the active forms of Rho, the conformational changes are induced, leading to the disruption of negative regulatory interactions between the kinase domain and the auto-inhibitory region, which then enhances autophosphorylation at the serine and threonine residues and elevates kinase activity to exogenous substrates (Ishizaki *et al.*, 1996; Leung *et al.*, 1996). In the

context of apoptosis, caspase 3 cleaved and removed the auto-inhibitory carboxyl terminal of ROCK1, resulting in constitutive ROCK1 activity (Sebbagh *et al.*, 2001). ROCK2 is activated similarly by Granzyme B-mediated cleavage, that concomitantly result in caspase 3 and thereby ROCK activation (Sebbagh *et al.*, 2005). Both of these two Rho-independent manners lead to the constitutively active ROCK activity, and then result in actin-myosin contraction, membrane blebbing, and apoptotic body formation (Sebbagh *et al.*, 2001, Sebbagh *et al.*, 2005). The activation of ROCK proteins could phosphorylate many different downstream effectors involved in many biological activities. Due to the similarity of the kinase domains of ROCK1 and ROCK2, the two isoforms possibly phosphorylate several common substrates. ROCK signaling pathway has been reported in many different cellular functions of Rho, and the ROCK-dependent actomyosin contraction is typically manifested in two biological phenomena: cytokinesis and blebbing in the apoptotic cells (Coleman and Olson, 2002; Amano *et al.*, 2010; Ohgushi *et al.*, 2010; Thumkeo *et al.*, 2013). ROCK phosphorylates intermediate filaments beneath the cleavage furrow and thereby promotes cytokinesis (Kosako *et al.*, 1997; Goto *et al.*, 1998). During the apoptosis phase, caspase-3 cleaves ROCK1 to remove the auto-inhibitory C-terminal domain, which results in constitutive ROCK1 activation and subsequent induction of plasma membrane blebbing through MLC phosphorylation. (Coleman *et al.*, 2001; Sebbagh *et al.*, 2001; Sebbagh *et al.*, 2005). However, the precise timing of ROCK activation has not been reported due to technical difficulty of its measurements.

### **1-3 FRET biosensor**

Genetically-encoded biosensors based on Förster/fluorescence resonance energy transfer (FRET) have been developed outstandingly in the past several years. FRET has been widely used as a spectroscopic technique in all applications of fluorescence, including medical diagnostics, DNA analysis, optical imaging and for various sensing properties (Oldach and Zhang, 2014; Miyawaki and Niino, 2015). Molecular activities in human body are highly dynamic and can occur locally in sub-cellular compartments. And even in the same tissue, the state of the cells is quite different. Therefore, quantitative information based on FRET technique is critical for the understanding of biological activity.

Conventionally, FRET-based biosensors are composed of three main parts: the

fluorophore pair, the linker and the recognition domain. First, the FRET efficiency is decided by the fluorophore pair. The commonly used fluorescent protein FRET pairs consisted of Cyan Fluorescent Protein (CFP) as the donor and Yellow Fluorescent Protein (YFP) as the acceptor. However, several drawbacks of these two pairs were discovered. CFP has low brightness, a four-fold lower brightness than its counterpart YFP, and YFP is much weak resistant to the environmental conditions, especially the pH (Urrea *et al.*, 2008), the chloride concentration (Zhong *et al.*, 2014), and the amount of O<sub>2</sub> during chromophore formation (Potzker *et al.*, 2012). These issues have been addressed by mutations, producing many enhanced versions CFP like eCFP, and advanced versions of YFP Cerulean (Rizzo *et al.*, 2004) and mTurquoise (Goedhart *et al.*, 2010). The linker region also plays an important role in FRET-based biosensors, affecting the dipole orientation and the distance between fluorophores. Komatsu *et al.* has reported that a long and flexible linker reduced the basal FRET level and increased the efficiency of the FRET-based biosensors (Komatsu *et al.*, 2011). Finally and most importantly, the specificity of the biosensor is mostly decided by the recognition domain. Most FRET biosensors adopt peptide sequences from the known substrate proteins did not show very high FRET efficiency, and the technology to find consensus phosphorylation sequence for many protein kinases is urgent to develop (Imamura *et al.*, 2009; Hires *et al.*, 2008; Van der Krogt *et al.*, 2008; Nagai *et al.*, 2004).

Recent advances in the technique of FRET biosensors have led to popular application of FRET biosensor. Aoki *et al.* reported a stable gene expression method of FRET biosensor based on piggyBac transposon and overcame the limit that most FRET biosensors could only be expressed transiently in cells due to the difficulty of the stable expression of both CFP and YFP (Aoki *et al.*, 2012). And other advances in the techniques further widened the application of FRET biosensors, and paved the way for the generation of transgenic mice to express FRET biosensors (Kamioka *et al.*, 2012; Johnsson *et al.*, 2014). With two-photon excitation microscopy, the real-time activity of protein could be observed in various tissues of the transgenic mice, with the greatly improved signal-to-background ratio.

#### **1-4 Kinase-interacting substrate screening**

Even with an optimized backbone for the FRET biosensor (Komatsu *et al.*, 2011), the development of a FRET biosensor for protein kinases is still a time-consuming

pursuit, because many of the peptide sequences known to be phosphorylated by a given kinase do not reliably work in the context of a FRET biosensor. With the significant progress of sensitivity of LC/MS/MS to identify the proteins, a novel method called kinase-interacting substrate screening (KISS) was developed by using affinity beads coated with the protein kinases to identify phosphorylation sites (Amano *et al.*, 2015). The procedure is simply introduced as follows. First, the affinity beads were coated with the catalytic domain of Rho-kinase, and then incubated with rat brain lysate to form kinase–substrate complexes. The complexes were incubated with ATP in the presence of  $Mg^{2+}$  to promote phosphorylation. To confirm the phosphorylation of substrates, immunoblot analyses were performed by using anti–phospho-motif antibodies that can recognize pSer/pThr. In the presence of ATP, several bands were detected, whereas in the absence of ATP, only few bands were detected, indicating that the interacting proteins were efficiently phosphorylated by Rho-kinase. Next, the samples were digested with trypsin to produce phosphorylated peptides. The peptides were concentrated, and analyzed by LC/MS/MS. This method revealed that many identified phosphopeptide sequences shared the consensus sequence for Rho-kinase (Amano *et al.*, 2010). Because the method of KISS deduces the consensus sequence from a huge number of phospho-peptides identified by liquid chromatography tandem mass spectrometry, the peptide sequence may be used to develop FRET biosensors for protein kinases with high sensitivity. Here, I employed the consensus substrate sequence for ROCK identified by KISS technology, and found it could develop a FRET biosensor for ROCK with very high sensitivity and specificity. Using this FRET biosensor, I found that, ROCK was activated during cytokinesis, and after cytokinesis, and rapidly re-activated concomitant with the spreading of cells on the culture dishes. ROCK activity was also found to increase gradually during apoptosis.

## **Chapter 2**

### **Experimental Procedures**

## 2-1 Reagents

Blasticidin S was purchased from InvivoGen (San Diego, CA). EGF and cycloheximide were purchased from Sigma-Aldrich (St. Louis, MO). Rapamycin was obtained from LC Laboratories (Woburn, MA). Y27632 dihydrochloride was purchased from Cosmo Bio (Tokyo, Japan). GSK429286 and HA1077 were purchased from Tocris Bioscience (Bristol, UK) and Tokyo Chemical Industry (Tokyo, Japan), respectively. TNF- $\alpha$  was purchased from Toyobo Co., Ltd. (Osaka, Japan). Phorbol 12-Myristate 13-Acetate (PMA), Forskolin, and 3-isobutyl-1-methylxanthine (IBMX) were purchased from Wako Pure Chemical Industries Ltd. (Osaka, Japan).

## 2-2 FRET biosensors and plasmids

FRET biosensors were constructed as described previously using the optimized Eevee backbone (Komatsu *et al.*, 2011). From the N-terminus, the Eevee backbone consists of YPet, a spacer (Leu-Glu), the FHA1 domain of yeast Rad53, a spacer (Gly-Thr), the EV Linker, a spacer (Ser-Gly), a substrate peptide sequence of ROCK proteins, a spacer (Gly-Gly-Arg), enhanced CFP, a spacer (Ser-Arg), and a subcellular localization signal. The substrate peptide sequences are summarized in Table 1. The substrate sequence of Eevee-ROCK was modified in such a way that the Ser residue at the phosphorylation site was replaced by Thr and the residue at the +3 position from the said Thr was substituted with Asp for optimal FHA1 binding. In Eevee-ROCK-T/A, the phosphoacceptor of Thr was mutated to Ala. In the constructs Eevee-ROCK-NLS, Eevee-ROCK-pm (KRas), and Eevee-ROCK-pm (HRas), the C-terminal localization signal was substituted by the nuclear localization signal of the SV40 large T-antigen (PKKKRKV), the C-terminal region of human KRas (KMSKDGKKKKKSKTKCVIM), and the C-terminal region of human HRas (KLNPPDESGPGCMSCKCVLS), respectively. In the case of Eevee-ROCK-pm (Lyn) and Eevee-ROCK-mito, additional localization signals were N-terminally added; these were the first 13 amino acids of human Lyn kinase and the mitochondrial localization sequence of human phospholipase D6

**Table 1. ROCK phosphorylation sites used for FRET biosensors**

Plasmids	Target proteins	Peptide sequences*	Ref
3654NES	Protein phosphatase 1 regulatory subunit 12A (T696)	ARQSRRSpTQG[V/D]TLTD	(Wooldridge <i>et al.</i> , 2004)
3655NES	ARHGAP35/p190A RhoGAP (S1150)	LERGRKV[pT]IV[S/D]KPVL	(Mori <i>et al.</i> , 2009)
3656NES	Ezrin (T567)	QGRDKYKpTLR[Q/D]IRQG	(Tran Quang <i>et al.</i> , 2000)
4146NES	CONSENSUS	KRRNRRKpTLV[L/D]LPLD	(Amano <i>et al.</i> , 2015)
4149NES	TA mutant	KRRNRRK[T/A]LV[L/D]LPLD	

\*The letter p indicates a phospho-amino acid. Amino acid substitutions are shown in parenthesis.

Aspartate (D) and threonine (T) are introduced to meet the consensus sequence of the FHA1 domain.

The T/A substitution in 4149NES is for the negative control.

(MGRLSWQVAAAAAVGLALTLEALPWVLRWLRSSRRRRPRR). I used pCAGGS (Niwa *et al.*, 1991) and pPBbsr (Yusa *et al.*, 2009) for transient and stable expressions, respectively. Plasmids for RhoA and Raichu-RhoA, the FRET biosensor for RhoA, were reported previously (Yoshizaki *et al.*, 2003; Kurokawa and Matsuda, 2005).

For the concrete procedure to make Eevee-ROCK(NES) plasmid, the first step is to produce the linearized vector by using the restriction enzyme according to the manufacturer's protocol (Takara Bio Inc., Kusatsu, Japan). 1 µg plasmid Eevee-PKA (NES) (Figure 2) was incubated with 2 µL K buffer, 0.5 µL restriction enzymes Aor13 HI, 2 µL BSA and deionized distilled water (DDW) (total volume 20 µL) at 55 °C for 1 hour. The product was purified with PCR purification kit (QIAGEN, Hilden, Germany). 5 volumes (100 µL) of Buffer PB with pH indicator was added to 1 volume(20 µL) of the digest sample with mixing. A QIAquick spin column was placed in a provided 2 ml collection tube, and the sample was applied to the QIAquick column and centrifuged for 1 min at 15,000 rpm. After discarding the flow-through, the QIAquick column was washed with 0.75 ml Buffer PE with the addition of ethanol, and centrifuged 1 min at 15,000 rpm. After discarding the flow-through again, the QIAquick column was

placed back in the same tube, centrifuged for an additional 1 min at 15,000 rpm, and placed in a clean 1.5 ml microcentrifuge tube. To elute DNA, 13.5 µl DDW was added to the center of the QIAquick membrane. The column was stood for 1 min to increase DNA concentration, and centrifuged for 1 min at 15,000 rpm. After collecting the flow, 0.5 µL restriction enzymes NotI, 2µL H Buffer, 2 µL BSA, and 2 µL Triton were mixed to make a mixture of 20 µL, and incubated at 37 °C for 1 hour. Then the DNA fragment was isolated with 1% agarose gel electrophoresis.

The second step is to purify DNA Fragments from Agarose Gels with glass beads (QIAGEN, Hilden, Germany). First the gel slice containing the DNA fragment was excised using a clean razor blade and was cut as close to the DNA as possible to minimize the gel volume. After placing the gel slice into a 1.5 ml tube, 800 µL Buffer QX1 and 5 µL QIAEX II Suspension were added to the gel slice, and the gel mixture was incubated at 55°C for 10 min with mixing the tube by inversion every few minutes to facilitate the melting process, and to keep the silica powder in suspension. After spinning silica powder/DNA mixture at 15,000 rpm for 1 s to form a pellet, the supernatant solution was carefully removed and discarded. The pelleted silica powder/DNA complex was resuspended with an additional 300 µl of Buffer QX1 to dissolve any residual undissolved in agarose. Again, after spinning the silica powder/DNA mixture at 15,000 rpm for 1 s to form a pellet, the supernatant solution was carefully removed and the flow-through was discarded. 300 µL of PE Buffer (diluted with ethanol) was added, and the pellet was resuspended and spun at 15000 rpm for 1 s before discarding the supernatant. After the supernatant from the last wash has been removed, the tube was spun again before removing the remaining liquid with a pipette. The pellet was air-dried for 10 min to avoid the presence residual ethanol in the purified DNA solution, due to the reason that residual of ethanol in the DNA sample may inhibit downstream enzymatic reactions. The pellet was resuspended in 10 µL sterile deionized water before incubating the tube at 55°C for 5 min. after spinning the tube, the supernatant was removed while avoiding the pellet, and the recovered supernatant was placed into a fresh tube.

Finally, for the process of annealing, both complementary oligonucleotides (oligonucleotides –F: ccggaAAGAGAAGAAACAGAAGAAAGACCCTGGTGGACCTGCCTCTGGATggc;

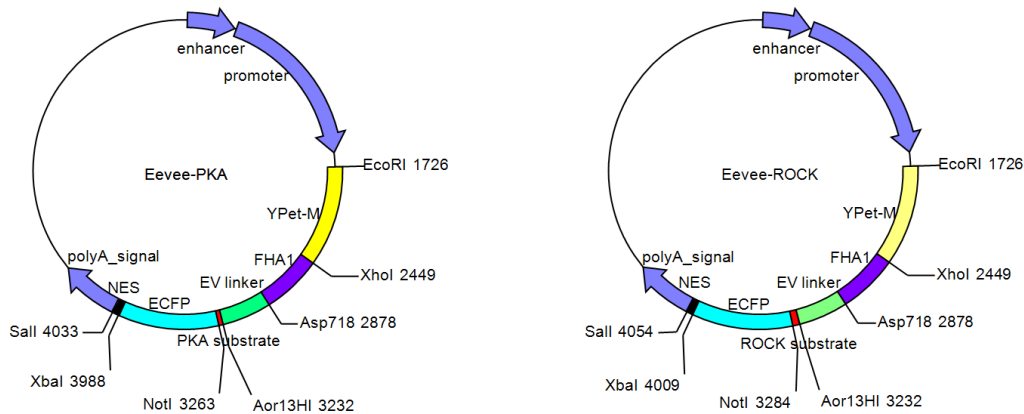


**Figure 2. Plasmid maps.** (A) Eevee-PKA biosensor; (B) Eevee-ROCK biosensor. Both FRET biosensors were based on the optimized Eevee backbone, which was comprised of, from the amino-terminus, YPet yellow fluorescent protein, the phospho-serine/threonine-binding FHA1 domain, the long flexible EV-linker, a substrate peptide for PKA/ROCK, and enhanced cyan fluorescent protein (CFP). We added a nuclear export signal (NES) at the C-terminus unless specified otherwise.

oligonucleotides –R:

ggccgccATCCAGAGGCAGGTCCACCAGGGTCTTTCTTCTGTTTCTTCTCTTt)

were resuspended at the concentration of 200  $\mu$ M, using Annealing Buffer (100mM Tris-HCl, pH8.0; 10mM EDTA, pH8.0; 1M NaCl). 5  $\mu$ L of both complementary oligos, 2  $\mu$ L annealing buffer, and 8  $\mu$ L DDW were mixed in a 1.5 ml microfuge tube. The tube was placed in a standard heatblock at 95  $^{\circ}$ C for 4 minutes, and then the heat block was removed from the apparatus and was allowed to cool to room temperature. The annealed oligos were diluted with nuclease-free water with the concentration being about 25nM. The annealed oligos were mixed with cut vector in molar ratios (vector: insert = 2:5) in a standard ligation reaction, and incubated at 16  $^{\circ}$ C for 30 min. Finally 2-3  $\mu$ L mixture was transformed into JM109 Competent cell .

### 2-3 Cell culture and transfection

HeLa cells were purchased from the Human Science Research Resources Bank (Sennanshi, Japan) and maintained in DMEM (Sigma-Aldrich, St. Louis, MO) supplemented with 10% fetal bovine serum (FBS; SAFC Biosciences, Lenexa, KS) at 37 $^{\circ}$ C, 5% CO<sub>2</sub>. HeLa cells were transfected with the plasmids by using 293fectin

(Invitrogen, San Diego, CA) according to the manufacturers' instructions. Before the transfection, HeLa cells were seeded in 35-mm glass bottom dish to be 30% confluent at transfection. Then 2  $\mu\text{g}$  of plasmid DNA in Opti-MEM<sup>®</sup> was diluted to a total volume of 50  $\mu\text{L}$  and 2  $\mu\text{L}$  of 293fectin<sup>™</sup> Reagent in Opti-MEM<sup>®</sup> to a total volume of 50  $\mu\text{L}$ , respectively. With gentle mixing and incubation for 5 minutes at room temperature. After the incubation, the diluted DNA was added to the diluted 293fectin<sup>™</sup> Reagent to obtain a total volume of 100  $\mu\text{L}$  with gentle mixing and incubation for 15 minutes at room temperature to allow DNA-293fectin<sup>™</sup> complexes to form. 100  $\mu\text{L}$  of the DNA-293fectin<sup>™</sup> complex was added to each well and mixed gently by rocking the plate back and forth. The cells were incubated in a 37 °C incubator for 24–48 hours before assaying for recombinant protein expression. For stable expression, the pPBsr-based expression vector and pCMV-mPBase (neo-) encoding the piggyBac transposase (Yusa *et al.*, 2009) were cotransfected and selected with 20  $\mu\text{g}/\text{ml}$  blasticidin S for at least 10 days. The rapamycin-inducible Akt or RhoA activation system was constructed as described previously (Suh *et al.*, 2006; Miura *et al.*, 2014). For the rapamycin-inducible RhoA activation system, pCX4bsr-3HA-FKBP-p63RhoGEF-DH encodes FKBP-p63RhoGEF-DH, which was comprised of the FK506-binding protein (FKBP) fused to the Dbl homology (DH) of the guanine nucleotide exchange factor p63RhoGEF as described previously (Van Unen *et al.*, 2015). pCX4puro-LDR encodes LDR, which was comprised of the FK506-rapamycin-binding (FRB) domain of mTOR fused to the myristoylation signal of Lyn (Suh *et al.*, 2006). Lentiviruses were prepared from the pCX4-derived plasmids and used to infect HeLa cells as described previously (Akagi *et al.*, 2003), generating HeLa-LDR/3HA-FKBP-p63RhoGEF-DH cells. After transfection of an expression plasmid for a FRET biosensor, cells were stimulated with 50 nM rapamycin to translocate p63RhoGEF to the plasma membrane. For the rapamycin-inducible Akt activation system, the procedure was similar, except that FKBP-iSH2 is comprised of the rapamycin-binding domain of the FK506-binding protein (FKBP) fused to the inter-*Src* homology 2 domain (iSH2) of the regulatory PI3K subunit p85 (Suh *et al.*, 2006; Miura *et al.*, 2014). Human ROCK1 cDNA was cloned from human cDNA library. Human ROCK2 cDNA (KIAA0619) was kindly provided from Kazusa DNA Research Institute (Chiba, Japan). ROCK1 cDNA and ROCK2 cDNA were subcloned into pEF-BOS-GST and pEGFP-c1 vectors, respectively. pEF-BOS-GST-bRho-kinase and

pEGFP-c1-bRho-kinase are expression vectors for bovine ROCK2/Rho kinase tagged with GST and GFP, respectively (Amano *et al.*, 2015).

#### **2-4 Time-lapse FRET imaging**

FRET imaging was performed as previously reported (Aoki and Matsuda, 2009). Cells were plated on 35-mm glass base dishes, transfected with plasmids, incubated for 24 h, and serum-starved for 3–6 h in phenol red-free M199 medium (Invitrogen, Carlsbad, CA) containing 20 mM HEPES (Invitrogen, Carlsbad, CA) and 0.1% BSA before imaging. Cells were imaged with an IX83 inverted microscope (Olympus, Tokyo, Japan) equipped with a PlanApo 60×/1.40 oil objective lens, a Cool SNAP K4 CCD camera (Roper Scientific, Tucson, AZ), a CoolLED precisExcite LED illumination system (Molecular Devices, Sunnyvale, CA), an IX2-ZDC laser-based autofocus system (Olympus), and an MD-XY30100T-Meta automatically programmable XY stage (SIGMA KOKI, Tokyo, Japan). The following filters used for the dual-emission imaging studies were obtained from Omega Optical (Brattleboro, VT): an XF1071 440AF21 excitation filter, an XF2034 455DRLP dichroic mirror, and an XF3075 480AF30 emission filter for CFP, and an XF3079 535AF26 emission filter for FRET. For the imaging of cytokinesis, HeLa cells stably-expressing Eevee-ROCK were time-lapse imaged with an LCV110 incubator-type inverted fluorescence microscope (Olympus, Tokyo, Japan) for two or three days. The filters used for the dual-emission imaging studies were obtained from Semrock (Rochester, NY): an FF02-438/24-25 excitation filter, an FF458-Di02-25x36 dichroic mirror, and an FF01-483/32-25 emission filter for CFP; an FF01-513/17 excitation filter and an FF01-542/27-25 emission filter for FRET. After background subtraction, FRET/CFP ratio images were created with Meta-Morph software (Universal Imaging, West Chester, PA), and represented in the intensity-modulated display mode. In the intensity-modulated display mode, eight colors from red to blue are used to represent the FRET/CFP ratio, with the intensity of each color indicating the mean intensity of FRET and CFP. For the quantification, the FRET and CFP intensities were averaged over the whole cell area, and the results were exported to Excel software (Microsoft Corporation, Redmond, WA). The FRET/CFP values before stimulation were averaged and used as a reference. The ratio of the raw FRET/CFP value to the reference value was defined as the normalized FRET/CFP value.

## 2-5 Small interfering RNA transfection

The control small interfering RNA (siRNA) was purchased from Dharmacon (Lafayette, CO). siRNA sequences of ROCK1 and ROCK2 were obtained from previous reports (Vega *et al.*, 2011; Iizuka *et al.*, 2012).

siROCK1-1 (5'-GAAGAAACAUCCCCUAUUC-3');

siROCK1-2 (5'-GCCAAUGACUUACUUAGGA-3');

siROCK2-1 (5'-GCAAUCUGUAAAUACUC G-3');

siROCK2-2 (5'-CAAACUUGGUAAAGAAUUG-3').

HeLa cells were transfected with small interfering RNA (siRNA) by Lipofectamine RNAi MAX (Invitrogen, Carlsbad, CA) according to the manufacturer's protocol. Before the transfection, HeLa cells were seeded in 24-well plate to be 60-80% confluent at transfection. Then 3  $\mu$ L Lipofectamine<sup>®</sup> RNAiMAX reagent was diluted in 50  $\mu$ L Opti-MEM<sup>®</sup> medium, while 10 pmole siRNA was diluted in 50  $\mu$ L Opti-MEM<sup>®</sup> medium, and the diluted siRNA was added to the diluted Lipofectamine RNAiMAX Reagent(1:1 ratio) with incubation of 5 minutes at room temperature. 50  $\mu$ L siRNA-lipid complex was added to seeded HeLa cells with the incubation of the cells for 24 hour or longer before the analysis of the transfected cells.

## 2-6 Western blotting

Cells were lysed in SDS sample buffer (62.5 mM Tris-HCl (pH 6.8), 12% glycerol, 2% SDS, 0.004% bromophenol blue and 5% 2-mercaptoethanol). The samples were separated by SDS-PAGE on SuperSep Ace 5–20% or SuperSep Ace 5–20% pre-cast gels (Wako Pure Chemical), and transferred to PVDF membranes (Merck Millipore, Darmstadt, Germany). After 60-min incubation with Odyssey blocking buffer (LI-COR Biosciences, Lincoln, NE, USA) at room temperature, the membranes were incubated for overnight at 4 °C with rabbit monoclonal anti-ERK1/2 antibody (1:1,000) (No. 9101; Cell Signaling Technology, Danvers, MA), rabbit monoclonal anti-ROCK1 antibody (1:1,000) (ab45171; Abcam, Cambridge, MA), rabbit monoclonal anti-ROCK2 antibody(1:1,000) (ab125025; Abcam), mouse Anti-ERK antibody (1:1,000) (No. 610123; BD biosciences, San Jose, CA) or mouse monoclonal anti-GFP antibody (1:8,000)(No. 632381, Clontech Laboratories, Inc., Mountain View, CA) . The immunoreactivities were visualized with IRDye 800CW-conjugated donkey anti-mouse IgG antibodies (1: 15,000; LI-COR) and IRDye 680LT-conjugated goat anti-rabbit IgG

antibodies (1: 15,000; LI-COR). All antibodies were diluted in Odyssey blocking buffer. Proteins were detected by an Odyssey Infrared Imaging System (LI-COR) and analyzed by using the Odyssey imaging software.

## **Chapter 3**

### **Results and Discussion**

### 3-1 Design of FRET biosensor for ROCK based on KISS

The FRET biosensor was based on the optimized Eevee backbone (Komatsu *et al.*, 2011), which was comprised of, from the amino-terminus, YPet yellow fluorescent protein, the phospho-serine/threonine-binding FHA1 domain, the long flexible EV-linker, a substrate peptide for ROCK, and enhanced cyan fluorescent protein (CFP) (Fig. 3A). I added a nuclear export signal at the C-terminus unless specified otherwise. The resulting FRET biosensor is expected to increase its FRET signal upon phosphorylation by ROCK (Fig. 3A).

As the substrate for ROCK, I first used the previously reported ROCK substrate sequences derived from protein phosphatase 1 regulatory subunit 12A(T696), ARHGAP35/p190A RhoGAP (S1150), and ezrin (T567) (Table 1). ROCK could phosphorylate the myosin phosphatase target subunit 1 (MYPT1) at Thr695 and inhibit myosin phosphatase activity (Feng *et al.*, 1999; Wooldridge *et al.*, 2004). A relatively high level of phosphorylation at Thr695 on MYPT1 was induced in serum-starved Swiss 3T3 cells by lysophosphatidic acid, thought to activate RhoA pathways, and this effect was blocked by ROCK inhibitor, Y27632 (Feng *et al.*, 1999). ROCK could also phosphorylate p190A RhoGAP at Ser1150 (Mori *et al.*, 2009). Small GTPase Rnd is known to be able to bind to p190A RhoGAP to enhance its activity toward GTP-bound RhoA, resulting in RhoA inactivation (Harada *et al.*, 2005; Wennerberg *et al.*, 2003). Phosphorylation of p190A RhoGAP by ROCK could impair Rnd binding and attenuate p190A RhoGAP activity. And ROCK inhibitor Y27632 could prohibit the process of sustained RhoA activation and p190A RhoGAP phosphorylation provoked by specific extracellular signals, endothelin-1 (ET-1). And the phosphomimic mutation of p190A RhoGAP weakened Rnd binding and RhoGAP activities. In summary, ROCK could phosphorylate p190A RhoGAP at Ser1150, attenuate p190A RhoGAP activity and induce the prolonged RhoA activation (Mori *et al.*, 2009). Finally, ROCK can phosphorylate the cytoskeletal linker protein ezrin C-terminus at T567 (Tran Quang *et al.*, 2000). ROCK inhibitor Y27632 could prohibit the relocalization of ezrin to dorsal actin-containing cell surface protrusions, the association of ezrin with the cytoskeleton and phosphorylation of T567 of ezrin. The ezrin mutant T567A could prevent the relocalization induced by activated RhoA or by ROCK, and inhibits RhoA-mediated contractility and focal adhesion formation (Tran Quang *et al.*, 2000). In the original

ROCK substrate consensus sequence, the threonine residue at the +3 position from the phosphothreonine was modified to aspartate to increase the affinity to the FHA1 domain.

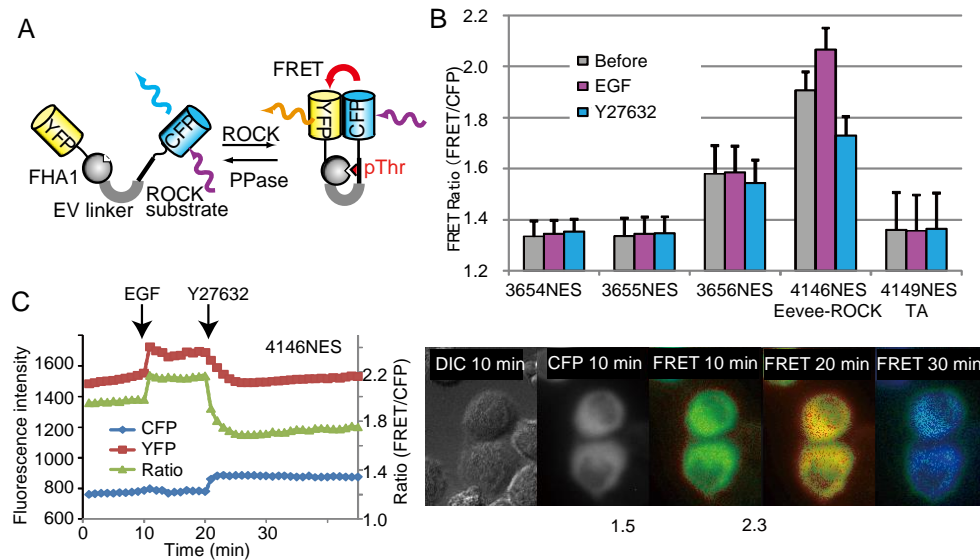


**Figure 3. Development of a FRET biosensor for ROCK, 4146NES/Eevee-ROCK.** (A) Mode of action of an intramolecular FRET biosensor for ROCK. Phosphorylation of the ROCK substrate peptide induces binding of the FHA1 domain to the substrate peptide, resulting in a conformational change and concomitant increase in FRET efficiency from the FRET donor CFP to the acceptor YFP. (B) HeLa cells expressing the FRET biosensor indicated at the bottom were serum-starved for more than 3 h and time-lapse imaged with an inverted epifluorescence microscope. Cells were stimulated with 10 ng/ml EGF at 10 min after the start of imaging, and then treated with 30  $\mu$ M Y27632, a ROCK inhibitor, at 20 min after the start of imaging. Images of DIC, CFP, and FRET (YFP fluorescence excited at 440 nm) were acquired at 1-min intervals. In each cell (N=24), the average FRET ratios from 0 to 10 min, 12 to 20 min, and 22 to 30 min were used to represent values before stimulation and after EGF and Y27632 stimulation. (C) Shown are actual time courses of CFP, FRET, and FRET/CFP values and representative images for 4146NES/Eevee-ROCK. FRET images are shown in the intensity-modulated display mode with the ratio range on the bottom. Scale bar, 20  $\mu$ m.

These FRET biosensors were transiently expressed in HeLa cells and time-lapse imaged to examine the response to 10 ng/mL EGF and 30  $\mu$ M ROCK inhibitor, Y27632. However, the developed FRET biosensors, 3654NES and 3655NES totally did not respond to either EGF or ROCK inhibitor Y27632. And the biosensor 3656NES present

very weak respond to the treatment of EGF and ROCK inhibitor Y27632(Fig. 3B). Next, I used the consensus substrate sequence of ROCK, which was identified by the KISS technology (Table 1). Similarly, the threonine residue at the +3 position from the phosphothreonine was modified to aspartate to increase the affinity to the FHA1 domain. In HeLa cells expressing the resulting FRET biosensor 4146NES, the FRET ratio was significantly increased around 8% upon EGF stimulation and decreased around 16% by Y27632 (Fig. 3B). The increase in the FRET ratio was caused by the increase in YFP intensity and decrease of CFP intensity as anticipated (Fig. 3C). Finally, the requirement of phosphorylation was confirmed by using 4149NES, in which the threonine at the phosphorylation site was substituted for alanine. The mutant did not respond to either EGF or Y27632 (Fig. 3B). Taken together, these results showed that 4146NES could be used as a ROCK biosensor and, therefore, I renamed 4146NES as Eevee-ROCK.

### **3-2 Specificity and sensitivity of Eevee-ROCK**

I next characterized the specificity of sensitivity of Eevee-ROCK. HeLa cells expressing Eevee-ROCK was also treated with stimulators of RhoA, 5% serum and 10  $\mu$ M lysophosphatidic acid (Fig. 4A). EGF could enhance ROCK activity most strongly, followed by serum, and lysophosphatidic acid. I also investigated the specificity of 4146NES by another ROCK inhibitor, GSK429286, and obtained essentially the same results as by Y27632 (Fig. 4B). Because all of these stimulators used here also activate ERK MAP kinase, I excluded the involvement of ERK by pretreatment with the MEK inhibitor U0126 (Fig. 4C). As expected, U0126 pre-treatment did not affect EGF-induced activation or Y27962-induced suppression of the ROCK activity.

To further confirm that Eevee-ROCK monitored ROCK activation, I applied the rapamycin-inducible RhoA activation system. This system employs two fusion proteins, FKBP-p63RhoGEF-DH, which was comprised of the FK506-binding protein (FKBP) fused to the Dbl homology (DH) of the guanine nucleotide exchange factor p63RhoGEF (Van Unen *et al.*, 2015) and LDR which was comprised of the FK506-rapamycin-binding (FRB) domain of mTOR fused to the myristoylation signal of Lyn (Suh *et al.*, 2006). Stimulation with rapamycin leads to rapid translocation of FKBP-p63RhoGEF-DH to the membrane-anchored LDR via hetero-dimerization of FKBP and FRB (Fig. 5A). The translocation of p63RhoGEF is expected to activate RhoA, and thereby ROCK. Indeed, the FRET/CFP ratio of Eevee-ROCK rapidly

increased upon stimulation with rapamycin, which could be prohibited by Y27632 as expected (Fig. 5B and 5C). Thus, Eevee-ROCK could faithfully monitor the RhoA activation induced by a Rho GEF.

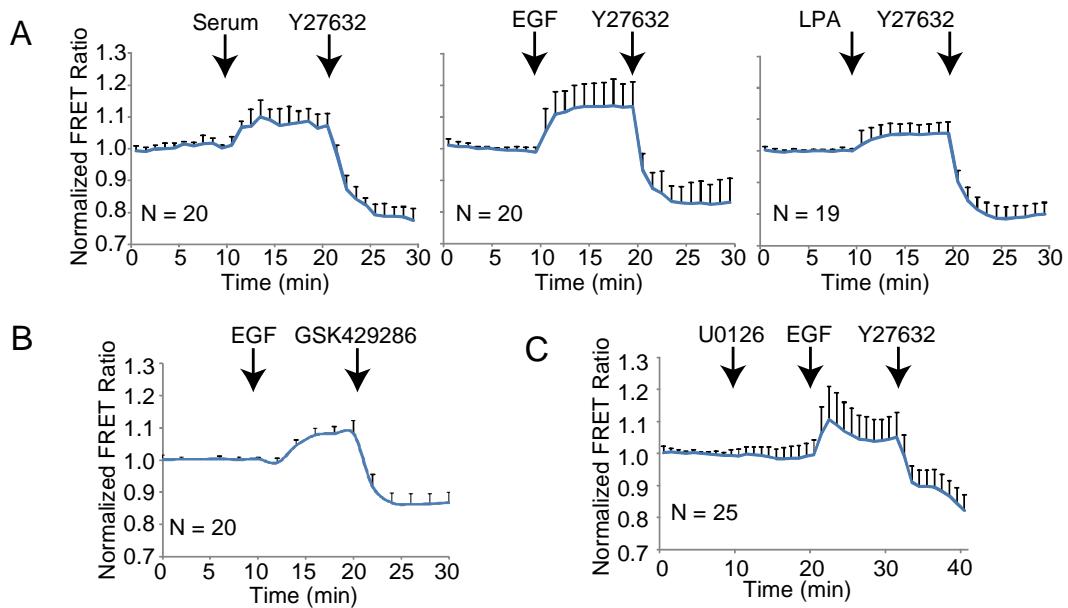


**Figure 4. Characterization of Eevee-ROCK.** (A) HeLa cells expressing Eevee-ROCK were serum-starved for more than 3 h and time-lapse imaged with an inverted epifluorescence microscope. Cells were stimulated with 5% serum, 10 ng/ml EGF, or 10  $\mu$ M LPA at 10 min after the start of imaging, and then treated with 30  $\mu$ M ROCK inhibitor Y27632, at 20 min after the start of imaging. Images of DIC, CFP, and FRET (YFP fluorescence excited at 440 nm) were acquired at 1-min intervals. The FRET/CFP ratio was normalized by the averaged FRET/CFP value before stimulation. (B) HeLa cells expressing Eevee-ROCK were stimulated with 10 ng/ml EGF and treated with 10  $\mu$ M GSK429286, another ROCK inhibitor. (C) HeLa cells expressing Eevee-ROCK were treated with the MEK inhibitor U0126 (10  $\mu$ M) at 10 min, EGF (10 ng/ml) at 20 min, and Y27632 (30  $\mu$ M) at 30 min after the start of imaging. Bars are the S.D. The numbers in the panels indicate the numbers of analyzed cells.

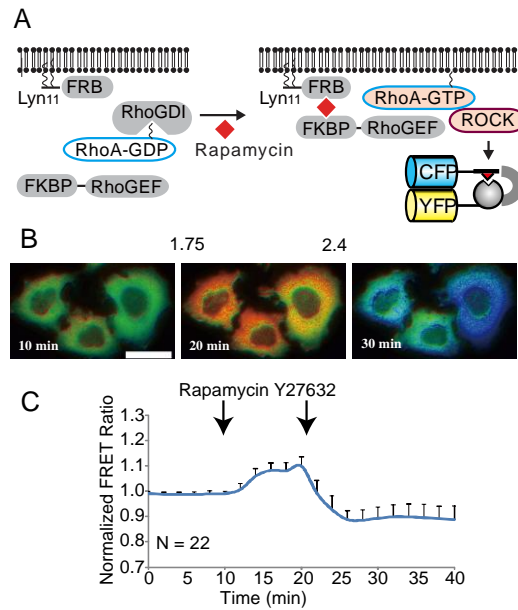


**Figure 5. Rapamycin-inducible RhoA activation.** (A) Schematic representation of the rapamycin-inducible ROCK activation. (B, C) HeLa cells expressing Eevee-ROCK were serum-starved for more than 3 h and time-lapse imaged with an inverted epifluorescence microscope. Cells were stimulated with 50 nM rapamycin at 10 min after the start of imaging, and then treated with 30  $\mu$ M ROCK inhibitor Y27632, at 20 min. Images of DIC, CFP, and FRET (YFP fluorescence excited at 440 nm) were acquired at 2-min intervals. Representative images of FRET/CFP (B) and the mean normalized FRET/CFP ratios (C) are shown with the S.D. Scale bar, 20  $\mu$ m.

Next I examined the response of Eevee-ROCK against stimulators specific to AGC kinases, like Akt, PKA, and PKC in the presence of ROCK inhibitor, Y27632. AGC kinases, which are named after 3 representative kinases, the cAMP-dependent protein kinase (PKA), the cGMP-dependent protein kinase (PKG) and the protein kinase C (PKC), are important regulatory enzymes that change the properties of a substrate by attaching a phosphate group to Ser, Thr residues. The AGC kinase family contains 60 members, including some intensely examined protein kinases, such as Akt, S6K, RSK, MSK, PDK1 and ROCK (Pearce et al., 2010). AGC kinases are involved in diverse and important cellular functions and their mutation and/or dysregulation contributes to the

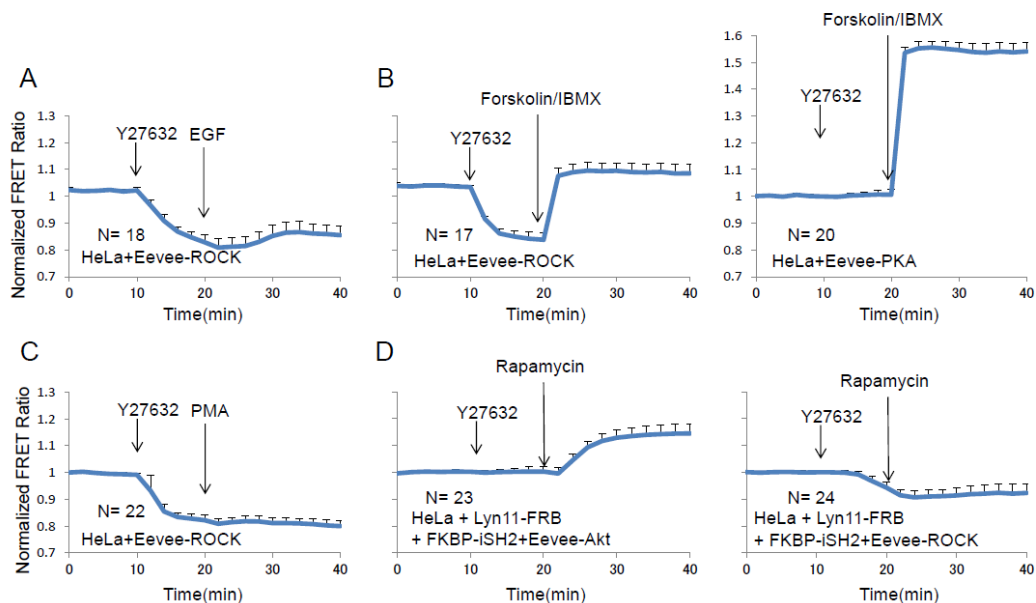


**Figure 6. Response of Eevee-ROCK against stimulators specific to other AGC kinases.** HeLa cells expressing the indicated plasmids were serum-starved for more than 3 h and time-lapse imaged. Cells were pretreated with 30  $\mu$ M Y2763 at 10 min, and stimulated with 10 ng/ml EGF, 1  $\mu$ M Forskolin/50  $\mu$ M IBMX, 1  $\mu$ M PMA, or 50 nM rapamycin at 20 min after the start of imaging. Images of DIC, CFP, and FRET (YFP fluorescence excited at 440 nm) were acquired at 2-min intervals. The mean normalized FRET/CFP ratios are shown with the S.D.

pathogenesis of many human diseases such as cancer, diabetes, obesity, neurological disorders, inflammation and viral infections(Arencibia *et al.*, 2013).

As expected from the results of Fig. 3, with the pre-treatment of Y27632, EGF barely increased the FRET/CFP ratio of Eevee-ROCK and the activity of ROCK(Fig. 6A). Unexpectedly, I observed the response of Eevee-ROCK to forskolin/IBMX, which increases cytoplasmic cyclicAMP level, and significantly enhance FRET/CFP ratio of Eevee-PKA, suggesting that Eevee-ROCK could be phosphorylated by PKA, too (Fig. 6B). Phorbol 12-myristate 13-acetate (PMA), known as a potent stimulator of PKC did not increase in the FRET/CFP ratio of Eevee-ROCK(Fig. 6C). Finally I analyzed the stimulation of Akt with rapamycin-inducible system. I applied the rapamycin-inducible

PI3K activation system to Eevee-iAkt (Suh *et al.*, 2006; Miura *et al.*, 2014), similar with the rapamycin-inducible RhoA activation system. This system employs two fusion proteins, the rapamycin-binding domain of the FK506-binding protein (FKBP) fused to the inter-*Src* homology 2 domain (iSH2) of the regulatory PI3K subunit p85 (FKBP-iSH2) and the FK506-rapamycin-binding (FRB) domain of mTOR fused to the myristoylation signal of *Lyn* (Lyn11-FRB) (Suh *et al.*, 2006; Miura *et al.*, 2014). Stimulation with rapamycin, leads to rapid translocation of FKBP-iSH2 to the membrane-anchored Lyn11-FRB via hetero-dimerization of FKBP and FRB. According to the translocation, the catalytic subunit of PI3K, p110, is recruited to the plasma membrane where it converts PI(4,5)P<sub>2</sub> to PI(3,4,5)P<sub>3</sub>. Rapamycin-induced Akt activation rapidly increased the FRET/CFP ratio of Eevee-iAkt (Miura *et al.*, 2014) but failed to increase the FRET/CFP ratio of Eevee-ROCK (Fig. 6 D). Taken together, Eevee-ROCK can be phosphorylated by PKA to some extent, but not by PKC or Akt.

### **3-3 Effect of siRNA-mediated silencing of ROCK expression and RhoA mutants on the FRET ratio of Eevee-ROCK**

To confirm the specificity of Eevee-Rock, I knocked down ROCK1 and ROCK2 by small interfering RNA (siRNA). The lysates were subjected to immunoblotting by using anti-ROCK1, anti-ROCK2, and anti-ERK antibodies. The specificity of the anti-ROCK antibodies was examined by the reactivity to recombinant ROCK1 and ROCK2 (Fig. 7A). The anti-ROCK1 antibody used in this study cross-reacted with ROCK2/Rho kinase; whereas the anti-ROCK2 antibody detected only ROCK2. In agreement with this specificity, the mixture of two siRNAs against ROCK1 partially decreased the band detected by anti-ROCK1 antibody (Fig. 7B). Meanwhile, the mixture of two siRNAs against ROCK2 decreased not only the band detected by anti-ROCK2 antibody but also the band detected by ROCK1. The mixtures of all four siRNAs almost completely diminished the bands detected by anti-ROCK1 antibody and anti-ROCK2 antibody.

Therefore, I concluded that the anti-ROCK1 antibody cross-reacted with ROCK2. Under this condition, knockdown of ROCK1 did not affect the FRET ratio, whereas knockdown of ROCK2 decreased the FRET ratio modestly. Knockdown of both ROCK1 and ROCK2 markedly decreased the FRET ratio, indicating that both ROCK1 and ROCK2 contributed to the basal FRET signal in HeLa cells (Fig. 7C).

To further confirm the contribution of RhoA to the basal FRET signal of Eevee-ROCK, the dominant negative RhoA (RhoA-T19N) and the constitutively activated RhoA (RhoA-F30L) were expressed in the Eevee-ROCK-expressing HeLa cells. The expression vector carries an ERed fluorescent protein tagged to a nuclear localization signal as a marker (Fig. 7D). The FRET ratio was decreased by RhoA-T19N and increased by RhoA-F30L, indicating that the FRET ratio of Eevee-ROCK was correlated with RhoA activity, supporting the notion that Eevee-ROCK served as the ROCK biosensor (Fig. 7E). Note that cells that did not express ERed-NLS in the RhoA-T19N-transfected or RhoA-F30L-transfected dish exhibited FRET/CFP ratios similar to cells transfected with empty vector.

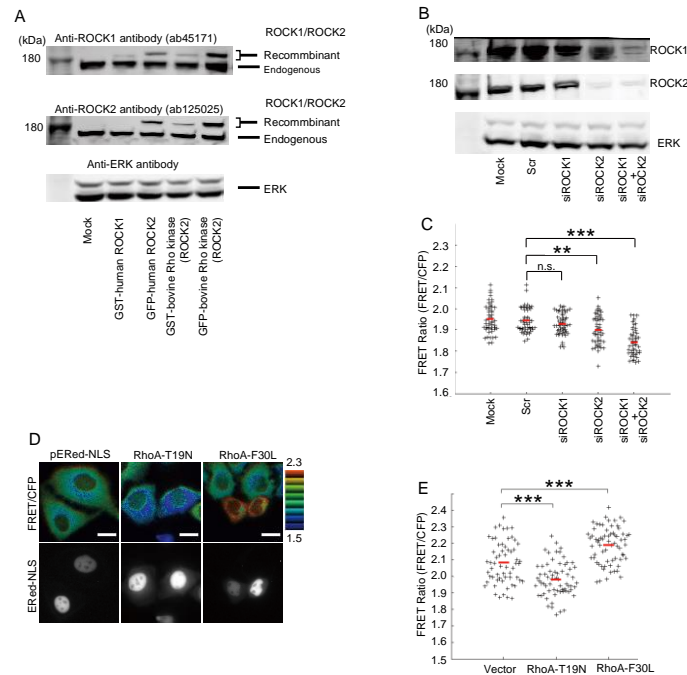


**Figure 7. Effect of ROCK1 and/or ROCK2 depletion and expression of RhoA mutants on Eevee-ROCK.** (A) HeLa cells were mock-transfected or transfected with the plasmids for GST-tagged human ROCK1, GFP-tagged human ROCK2, GST-tagged bovine Rho kinase/ROCK2, and GFP-tagged bovine Rho kinase/ROCK2. Cells were analyzed by SDS-PAGE and immunoblotting with anti-ROCK1 antibody, anti-ROCK2 antibody and anti-ERK antibody. (B, C) HeLa cells expressing Eevee-ROCK were mock-transfected or transfected with scramble siRNA (scr) or siRNAs against ROCK1 and/or ROCK2. Cells were analyzed by immunoblotting with antibodies against ROCK1, ROCK2, and ERK (B). The FRET ratio (FRET/CFP) was calculated for 52 cells under each condition, and the resulting ratios are shown in a bee swarm plot (C). Red bars represent the averages. Results of unpaired Student's *t*-tests are shown. n.s., not significant ( $p > 0,05$ ); \*\* $p < 0,01$ ; \*\*\* $p < 0,001$ . (D, E) HeLa cells were transfected with the empty vector pERed-NLS, the expression plasmid for the dominant negative mutant pERed-NLS-RhoA-T19N, or the expression plasmid for the constitutively active mutant pERed-NLS-RhoA-F30L. Fluorescence images were acquired and FRET/CFP values were calculated. Shown in (D) are representative images of the FRET/CFP ratio and the nuclear ERRed fluorescent protein, which was used to identify transfected cells. The obtained bee swarm plot is shown in (E). Scale bars, 20  $\mu\text{m}$ .

### 3-4 Effect of subcellular localization on ROCK activity

For the analysis of subcellular ROCK activity, various localization sequences were added to the Eevee-ROCK biosensor as reported for Akt biosensors (Miura *et al.*, 2014).

Transport of proteins between the nucleus and the cytoplasm is mostly facilitated by specific soluble carrier proteins, which are referred to as “karyopherins”, with those involved in import and export termed “importins” and “exportins” (Radu *et al.*, 1995; Gorlich *et al.*, 1994; Stade *et al.*, 1997), respectively. The direction of nuclear–cytoplasmic transport is dictated by nuclear targeting signals within the cargo proteins. Nuclear localization signals (NLSs) direct proteins import into the cell nucleus through the nuclear pore complex using nuclear transport, whereas nuclear export signals (NESs) direct export of proteins from the nucleus to the cytoplasm (Kalderon *et al.*, 1984; Lanford and Butel, 1984). NLS and NES have been well characterized. The classical NLSs for nuclear protein import are exemplified by the SV40 large T antigen NLS (126PKKKRRV132) (Robbin *et al.*, 1991; Dingwall and Laskery, 1991), and NESs, rich in leucine residues, were first identified in the proteins HIV-1 Rev and cyclical AMP-dependent protein kinase inhibitor (Fischer *et al.*, 1995; Wen *et al.*, 1995). In this study I used these two consensus signal sequences for transport of Eevee-ROCK biosensor. When Eevee-ROCK was localized to the nucleus, both serum-induced activation and Y27632-mediated inhibition were markedly attenuated (Fig. 8). Y27632-mediated suppression might be the reason that Y27632 did not arrived at the nuclear.

Association with cellular membranes by virtue of a series of post-translational modifications of their C-terminal CAAX sequences is required for the biological activity of Ras family proteins (Clarke, 1992). This processing is directed by a conserved CAAX motif at the C-terminus that contains an invariant cysteine as the fourth to last residue. CAAX sequences direct prenylation by cytosolic prenyltransferases, farnesyltransferase or geranylgeranyl-transferase I. These enzymes catalyze the addition of a 15-carbon

farnesyl or a 20-carbon geranylgeranyl lipid to the CAAX cysteine (Casey and Seabra, 1996). After prenylation, Ras proteins become substrates for a protease designated Ras converting enzyme 1 (Rce1) that removes the AAX amino acids of the CAAX sequence (Boyartchuk *et al.*, 1997; Otto *et al.*, 1999).

The new C-terminal prenyl cysteine then becomes a substrate for the final CAAX processing enzyme, isoprenylcysteine carboxyl methyltransferase (Icmt) that methyl esterifies the  $\alpha$  carboxyl group (Clarke *et al.*, 1988). The end result of these modifications is to remodel a hydrophilic C-terminus into one that is hydrophobic. The CAAX sequence

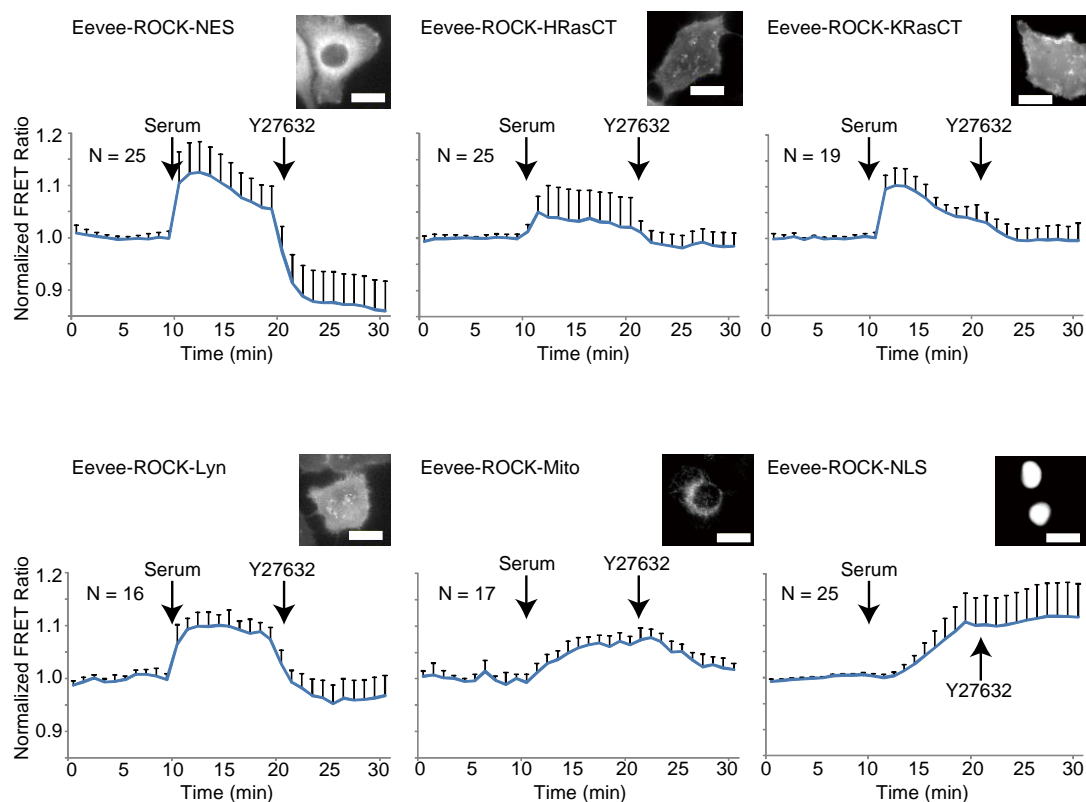


**Figure 8. Subcellular ROCK activity in HeLa cells.** Eevee-ROCK biosensors with subcellular localization signals were transfected into HeLa cells, which were serum-starved for more than 3 h, stimulated with 5% serum at 10 min, and then treated with 30  $\mu$ M Y27632 at 20 min after the start of imaging. Images of CFP and FRET were acquired at 1-min intervals with an inverted fluorescence microscope equipped with a CCD camera. Shown in the insets are representative CFP images. The FRET/CFP ratio was normalized by the averaged FRET/CFP value before stimulation. The normalized FRET/CFP ratios and S.D. are shown. The numbers in the panels are the numbers of analyzed cells. Scale bars, 20  $\mu$ m.

along with a polybasic motif from KRas provides anchoring to the non-raft plasma membrane, whereas the CAAX sequence with the adjacent palmitoylation sites from HRas and the N-terminal portion of Lyn kinase provide localization to raft regions of the plasma membrane (Prior *et al.*, 2001; Zacharias *et al.*, 2002). The HRas CAAX box additionally targets the sensor to the Golgi apparatus (Rocks *et al.*, 2005). Plasma membrane recruitment of the ROCK biosensor by the farnesylation signal of HRas or KRas attenuated the serum-induced increase in FRET ratio (Fig. 8). Moreover, I found that Y27632 did not decrease the FRET ratio any further than the basal level, indicating that the basal phosphorylation level was markedly suppressed when the biosensor was placed on the plasma membrane. Interestingly, plasma membrane targeting by the myristoylation signal of Lyn did not significantly perturb the serum-induced increase in FRET ratio.

For targeting to the mitochondrial outer membrane, the mitochondrial localization sequence of human phospholipase D6 was added (Choi *et al.*, 2006). When Eevee-ROCK was localized to the mitochondria, both serum-induced activation and Y27632-mediated inhibition were markedly attenuated (Figure 8). Taken together, these results showed that the localization of the FRET biosensor markedly affected its response, strongly suggesting that the regulation of ROCK may be subject to the subcellular localization.

### **3-5 ROCK activation at M phase and early G1 phase**

ROCK is well known for their regulation of actin cytoskeletal structures. In addition, ROCK influences progression through the cell cycle and its loss leads to cell-cycle arrest. Depletion of ROCK1 and ROCK2 leads to severe defects in cell proliferation, which are also observed in the cells treated with ROCK inhibitors, H1152, GSK269962A, AT13148, GSK429286A and chroman1 or myosin II ATPase inhibitor blebbistatin (Kümper *et al.*, 2016). In addition, the ROCK inhibitor Y27632 could inhibit the proliferation of cells, like vascular smooth muscle cells (Seasholtz *et al.*, 1999), hepatic stellate cells (Iwamoto

*et al.*, 2000), prostatic smooth muscle cells (Rees *et al.*, 2003), glial cells (Sorensen *et al.*, 2003), spleen-derived primary and Jurkat T cells (Tharaux *et al.*, 2003), cardiac myocytes (Zhao and Rivkees, 2003), corneal stromal cells (Harvey *et al.*, 2004), HSQ-89 oral squamous carcinoma cells (Nishimaki *et al.*, 2004), atrial myofibroblast cells (Porter *et al.*, 2004), umbilical vein endothelial cells (Seibold *et al.*, 2004), chondrocytes (Wang *et al.*, 2004), C6 glioma cells (Cechin *et al.*, 2005), IMGE-5 gastric epithelial cells (He *et al.*, 2005), and CD34<sup>+</sup> hematopoietic stem cells (Vichalkovski *et al.*, 2005). ROCK inhibition was thought to affect cell proliferation due to a G1 arrest and block in cytokinesis (Kümper *et al.*, 2016).

With an LCV110 incubator-type inverted fluorescence microscope, I tested ROCK activity during cell cycle with Eevee-ROCK biosensor, and focused on cytokinesis and G1 phase. This would broaden our recognition of Rho and ROCK regulation of the cell cycle, which may help in the design of anticancer therapies that target this signaling pathway. I found that ROCK activity was increased rapidly upon entering into M phase and decreased at the completion of cytokinesis (arrows in Fig. 9A, B). Interestingly, ROCK activity rapidly increased again when the cells began to spread and adhere to the dish. After entering the G1 phase, the ROCK activity gradually decreased until M phase. To examine the contribution of ROCK to the increase in FRET/CFP ratio, I performed similar experiments in the presence of three ROCK inhibitors, Y27632, GSK429286, and HA1077 (Fig. 9B-D). All three inhibitors markedly decreased the FRET/CFP ratio during interphase. However, the inhibitors did not suppress the rapid increase in FRET/CFP ratio in M phase, indicating that kinases other than ROCK contributed to the increased FRET/CFP in M phase. Significant number of cells treated with the ROCK inhibitors failed to complete cytokinesis, generating binuclear cells (Fig. 9C, D).

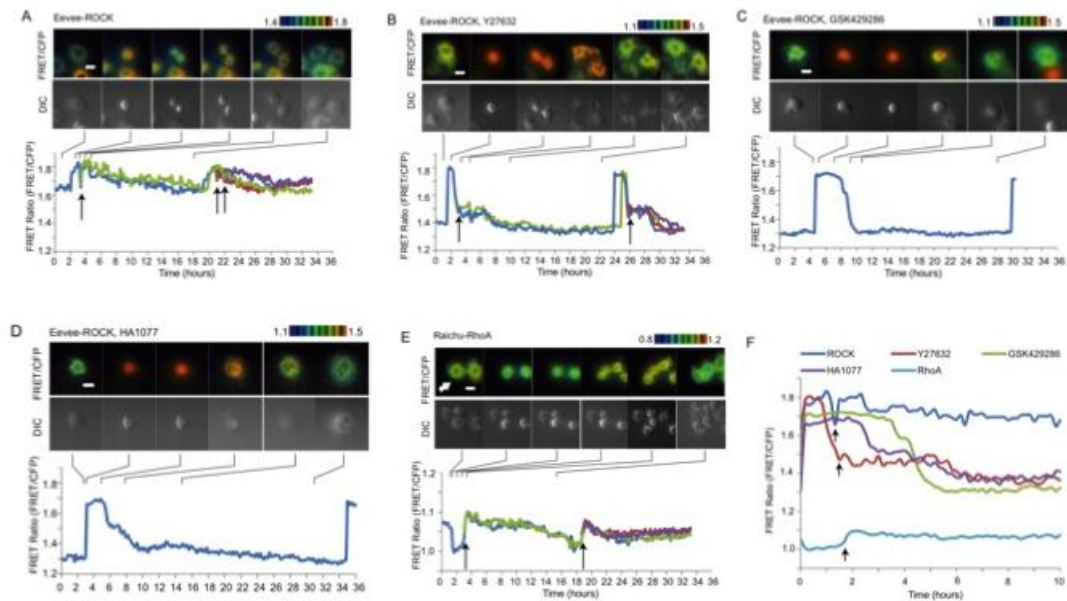


**Figure 9. ROCK activation before cytokinesis and during cell spreading.** (A-D) With an LCV110 incubator-type inverted fluorescence microscope, HeLa cells stably-expressing Eevee-ROCK were time-lapse imaged in the absence (A) or presence of ROCK inhibitors, 300  $\mu$ M Y27632 (B), 100  $\mu$ M GSK429286 (C), and 100  $\mu$ M HA1077 (D). Images were acquired every 10 min for two to three days. FRET/CFP ratio images and DIC images (upper panels) were acquired at the time points indicated on the lower panels. The FRET ratios (FRET/CFP) of a representative cell and its daughter cells were plotted against time (lower panels). The exposure times for CFP and FRET were 500 and 500 msec, respectively. Scale bar, 20  $\mu$ m. The arrows in the upper panels indicate the completion of cytokinesis (abscission). (E) HeLa cells stably-expressing Raichu-RhoA were time-lapse imaged as described. (F) Overlay of the time courses of FRET/CFP ratio changes. The origin was set to the nuclear breakdown at M phase.

Importantly, in the presence of ROCK inhibitors, the FRET/CFP ratio was not increased after the completion of cytokinesis, indicating that the increased FRET/CFP ratio after abscission (Fig. 9A) is due to ROCK activation. In agreement with this note, I observed that RhoA activity was initially decreased in M phase and increased during and after cytokinesis (Fig 9E) (Yoshizaki *et al.*, 2003). I did not observe any remarkable

changes of FRET/CFP ratio in HeLa cells expressing 3623NES(data not shown), in which the threonine residue was replaced with alanine on the background of the PKA biosensor, excluding the possibility that morphological changes caused the apparent fluctuation of the FRET/CFP ratio values (Fig. 9C). Taken together, ROCK appears to contribute to cell adhesion in the early G1 phase.

### **3-6 ROCK activation during apoptosis**

In the usual cellular context, ROCK is activated when the Rho binding domain (RBD) of ROCK binds to the active forms of Rho, inducing a conformational change and/or with promoting autophosphorylation within this region. No marked contraction and blebbing was produced due to the contribution of agonist-induced changes to the actin cytoskeleton with the cooperation of ROCK and other Rho-effector proteins, particularly mDia (Watanabe *et al.* 1999; Tominaga *et al.* 2000). However, in the context of apoptosis, caspase-mediated cleavage removes the putative autophosphorylation/auto-inhibitory domain, resulting in Rho-independent activation of ROCK1 (Coleman *et al.* 2001).

Next I therefore observed the timing of ROCK activation during apoptosis induced by TNF- $\alpha$  and cycloheximide (CHX). The FRET/CFP ratio of HeLa cells stably-expressing Eevee-ROCK was increased gradually for 3-4 h without remarkable morphological changes (Fig. 10A). Then the cells suddenly started to shrink, concomitant with a rapid surge and then a drop in the FRET/CFP ratio. These marked morphological changes occurred 208 +/- 27 min after the addition of TNF- $\alpha$  and CHX. After this period, the cells exhibited membrane blebbing without any increase in FRET/CFP ratio (Fig. 10C). When the cells were pre-treated with Y27632 and GSK429286 before TNF- $\alpha$  and cycloheximide (CHX), the FRET/CFP ratio remained low throughout the observation period (Fig. 10B). After several hours without remarkable morphological changes, the cells rapidly retracted as observed in the control cells. The striking difference was that the membrane blebbing in the ROCK inhibitor-treated cells was not as obvious as that in the control cells. The periods

between the addition of reagents and apoptosis in HeLa cells treated with Y27632 and GSK429286 were 265 +/- 51 and 282 +/- 56 min, respectively. Thus, inhibition of ROCK inhibited membrane blebbing and delayed the onset of, but did not prevent, apoptosis. These results consist with the previous report that, ROCK inhibitors did not affect biological events, like caspase activation, DNA fragmentation and release of cytochrome c from mitochondrial stores (Coleman *et al.* 2001). Another interesting observation was the rapid decrease in FRET/CFP ratio after the initiation of apoptosis. I speculated that the cleavage of the linker region might have caused this rapid decrease and tested the integrity of the probe by immunoblotting (Fig. 10D). Against our expectation, I detected only the intact Eevee-ROCK of 81.9 kDa, but not cleaved forms.

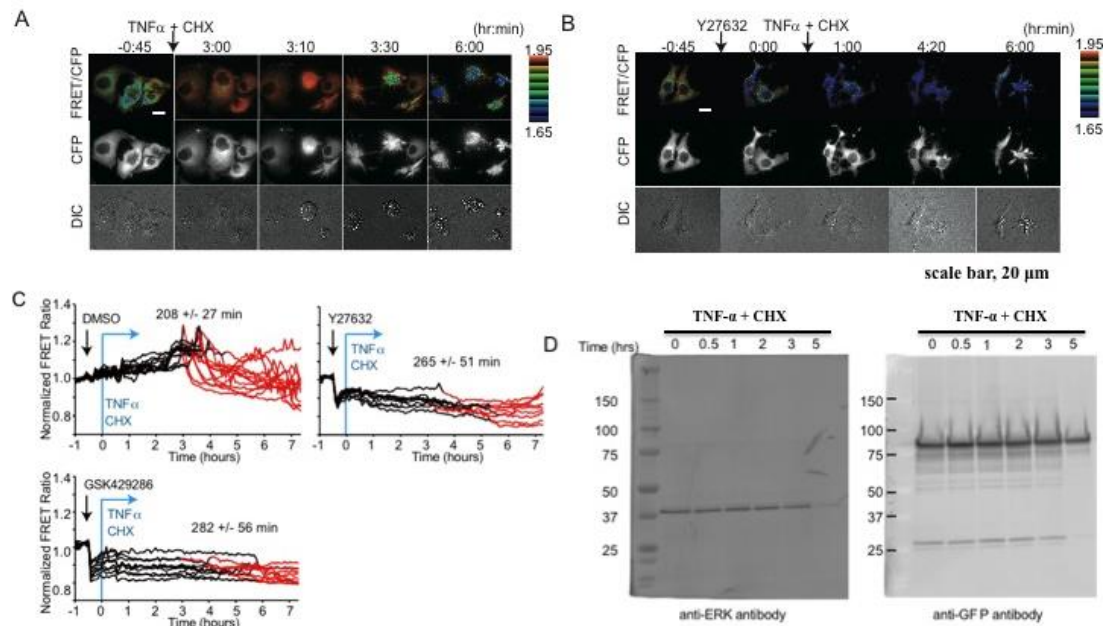


**Figure 10. ROCK activation during apoptosis.** HeLa cells stably-expressing Eevee-ROCK were time-lapse imaged with an inverted epifluorescence microscope. Images were acquired every 5 min for at least 8 h. DMSO as a solvent control, 30  $\mu$ M Y27632, or 10  $\mu$ M GSK429286 was added at 30 min after the start of imaging. For the induction of apoptosis, 10  $\mu$ g/mL TNF- $\alpha$  and 100  $\mu$ g/mL cycloheximide (CHX) were added at 60 min. Representative images of FRET/Ratio, CFP, and DIC images for the solvent control (A) and Y27632-treated cells are shown. Scale bars, 20  $\mu$ m. (C) Time courses of FRET/CFP ratios normalized to the first 30 min. The timing of apoptosis was determined by the nuclear membrane breakdown on the CFP images. Time points after apoptosis are shown by red lines. (D) In a parallel experiment, cells were lysed at the indicated time points and analyzed by immunoblotting with antibodies against ERK and GFP(Eevee-ROCK).

## **Chapter 4**

## **Conclusion**

The specificity of FRET biosensors for protein kinase activity depends on the kinase-specific substrate peptide (Sample *et al.*, 2014). Most, if not all, FRET biosensors adopt peptide sequences from the known substrate proteins, except for AKAR, a PKA biosensor, in which the PKA phosphorylation consensus sequence is used (Zhang *et al.*, 2001). In fact, the consensus phosphorylation sequence has not been known for many protein kinases, which forces developers to use the peptides known to be phosphorylated by the kinase of interest. In this study, I also attempted in vain to generate FRET biosensors for ROCK based on the phosphorylation sites derived from protein phosphatase 1, ARHGAP35(p190A RhoGAP), and ezrin (Tran Quang *et al.*, 2000; Wooldridge *et al.*, 2004; Mori *et al.*, 2009). In contrast, the consensus sequence for ROCK phosphorylation that was determined by the kinase-interacting substrate screening served as a sensitive and specific substrate for ROCK in the context of the FRET biosensor based on the Eevee backbone (Komatsu *et al.*, 2011). In KISS technology, the consensus sequences for phosphorylation are determined experimentally from a huge number of peptides (Amano *et al.*, 2015), which may underlie the high sensitivity and selectivity in the context of the FRET biosensor. Meanwhile, the substrate sequence used in Eevee-ROCK was found to be phosphorylated also by PKA, a member of AGC-family kinases. Furthermore, ROCK inhibitors failed to suppress robust increase in FRTE/CFP ratio in M phase (Fig. 9), indicating that kinases activated in M phase also phosphorylates Eevee-ROCK. Therefore, it should be kept in mind that the responses observed by using Eevee-ROCK should be validated in the presence of specific inhibitors of ROCK.

In this study, I used pCAGGS (Niwa *et al.*, 1991) and pPBbsr (Yusa *et al.*, 2009) for transient and stable expressions, respectively. The vector pCAGGS was constructed by introducing the CAG promoter, 3' part of rabbit globin gene including a polyadenylation signal, and an SV40 *ori* into pUC13 (Niwa *et al.*, 1991) for high-level production of proteins encoded by various genes and cDNAs in many cells (Gluzman, 1981; Gerard and Gluzman, 1985; Niwa *et al.*, 1991). In addition, pCAGGS directed high-level expression of various genes in all the tissues as far as examined in transgenic mice. However, the transient expression methods have a serious disadvantage. The expression levels will be reduced over a few days with the cell division, suggesting that sustained expression is beneficial to achieve reprogramming with a higher efficiency. Although retroviral delivery of the reprogramming factors is efficient and used widely,

the cells generated with retroviral vectors were found to have insertional mutations and were known to be tumorigenic. A non-mutated genome is an important requirement for protein expression. The piggyBac transposon-based technique could stably express the transgenes with efficiencies similar to the retroviral method and retain a non-mutated genome by removing the integrated piggyBac transposons from the host genome permanently without genetic alteration (Yusa *et al.*, 2009).

ROCK was reported to affect cell proliferation due to a G1 arrest and block in cytokinesis (Kümper *et al.*, 2016). ROCK activation elevates levels of cyclin A and cyclin D1, and decreases levels of p27 in NIH 3T3 fibroblasts (Croft and Olson, 2006). And the cell proliferation defects arising from abrogation of ROCK function lead to the decreased level of cell cycle proteins CDK1, Cyclin A and the cyclin-dependent kinase inhibitor CKS1, which was also observed by the treatment with myosin II inhibitor, blebbistatin (Kümper *et al.*, 2016). Cytokinesis is the final stage of cell division that generates two separate daughter cells through the actions of the actin-myosin-rich contractile ring. The role of the Rho/ROCK pathway in cytokinesis has been established by many research groups (Schwayer *et al.*, 2016). Importantly, ROCK accumulates at the cleavage furrow and phosphorylates several proteins, including the myosin regulatory light chain (MLC), during cytokinesis in several cultured cell lines (Kosako *et al.*, 2000). Because ROCK inhibitors failed to suppress the increased FRET/CFP ratio during M phase, the activation of ROCK in M phase could not be evidenced with Eevee-ROCK. A substrate sequence specific to ROCK or a method to target the FRET biosensor to ROCK may be required for this purpose. Although I failed to show ROCK activation during M phase, I found that, after the completion of cytokinesis, ROCK activity rapidly increased when cells spread and adhered to the dishes. Because ROCK plays critical roles in the formation of stress fibers and focal contacts in interphase (Narumiya *et al.*, 2009), the reactivation of ROCK in early G1 phase is reasonable. In agreement with this observation, I reported previously that RhoA activity was decreased in M phase and increased during and after cytokinesis in HeLa cells (Yoshizaki *et al.*, 2003; Yoshizaki *et al.*, 2004).

The role of ROCK as a critical effector of the membrane blebbing, a hallmark of apoptotic cells, is well recognized (Coleman and Olson, 2002). During the execution phase, caspase-mediated cleavage and activation of ROCK1 induce actomyosin contraction and dynamic membrane blebbing (Coleman *et al.*, 2001; Sebbagh *et al.*,

2001). As expected, I observed the rapid increase in the FRET ratio before the contraction of apoptotic cells (Fig. 10A). However, the rapid decrease of FRET ratio during the execution phase of apoptosis was unexpected. Cleavage of the linker region was the likely explanation; however, I failed to detect the cleaved FRET biosensor (Fig. 10D). The question of whether the decrease in FRET ratio indeed reflects a decrease in ROCK activity awaits further analysis. The role played by ROCK during apoptosis has been attracting more interest because the ROCK inhibitor Y27632 was discovered to prevent apoptosis of human embryonic stem cells (hESCs) during passage (Watanabe *et al.*, 2007). Further studies revealed that RhoA-dependent activation of ROCK causes apoptosis of hESCs during the passage (Chen *et al.*, 2010; Ohgushi and Sasai, 2010; Walker *et al.*, 2010). This apoptosis of hESCs critically differs from that triggered by death receptors such as the TNF receptor in the time lag between the membrane blebbing and nuclear breakdown of the apoptotic cells. In hESCs, membrane blebbing continues for several hours before cell death, whereas in the death receptor-mediated cell death, the membrane blebbing is immediately followed by the cell death (Ohgushi and Sasai, 2011). In agreement with these previous reports, I found that ROCK activation and membrane blebbing were observed immediately before the nuclear breakdown of the cells treated with TFN- $\alpha$  and CHX (Fig. 10). I also noticed that the timing of cell contraction and nuclear breakdown was delayed approximately 1 h in the ROCK inhibitor-treated cells. Therefore, the ROCK-mediated activation of mitochondria may accelerate the apoptosis induced by TFN- $\alpha$  and CHX (Ohgushi and Sasai, 2010).

FRET is undoubtedly a powerful bioanalytical technique capable of making precise intramolecular measurements in a variety of experimental platforms and formats. Recent dramatic improvements in the development of increased spatial resolution, distance range and sensitivity have enhanced the strength of this technique and resulted in its increasing popularity. Despite the diverse applications of FRET, FRET-based sensors still face many challenges, like the needs for high fluorescence resolution and improved specificity (Chaudhuri *et al.*, 2001). Additionally, FRET photodamages cells or photobleaches the fluorophores, and it has also auto-fluorescence background (Xia and Rao, 2009). Bioluminescence resonance energy transfer (BRET)-based biosensors, an alternative to FRET in which a light-emitting enzyme is used instead of an external light source for donor excitation, could avoid the disadvantage of FRET (Prinz *et al.*,

2006; Lohse *et al.*, 2008; Jensen *et al.*, 2009). The major donor of BRET is based on Renilla reniformis luciferase (Rluc) or its different variations, whereas the acceptor fluorophore is the derivative of green fluorescent protein (GFP) from the jellyfish *Aequorea victoria* (Prasher *et al.*, 1992; Xu *et al.*, 1999; Xia and Rao, 2009). The light source for the donor is a chemical substance that is converted by Rluc, and then the energy is transferred to the acceptor fluorophore, applying the same rules as for FRET (Hamdan *et al.*, 2005; Loening *et al.*, 2006; De *et al.*, 2007;). The demand for highly sensitive nonisotopic and noninvasive bioanalysis systems for biotechnology applications, such as those needed in clinical diagnostics, food quality control, and drug delivery, has driven research in the use of FRET and BRET for biological and chemical applications (Herzberg, 2009; De *et al.*, 2009; Dragulescu-Andrasi *et al.*, 2011; Saito *et al.*, 2012; Robinson *et al.*, 2014). Development of FRET and BRET based sensing system for practical application is a challenge, requiring an interdisciplinary outlook. Future progress of research in the area of FRET and BRET sensor is dependent upon the close collaboration of physicists, chemists, biologists, material scientists and computing specialists (Lohse *et al.*, 2008; Jensen *et al.*, 2009).

In summary, I developed a novel genetically-encoded FRET biosensor specific to ROCK activity, Eevee-ROCK, and demonstrated its versatility as a tool for examining the temporal activity changes of ROCK during the cell cycle and apoptosis. The successful development and application of Eevee-ROCK has validated the usefulness of the substrate peptides identified by means of KISS technology, and will encourage researchers to develop FRET biosensors for the protein kinases of their interest.

## Bibliography

- Akagi, T., Sasai, K., and Hanafusa, H. 2003. Refractory nature of normal human diploid fibroblasts with respect to oncogene-mediated transformation. *Proc. Natl. Acad. Sci. U.S.A.*, **100**:13567-13572.
- Amano, M., Hamaguchi, T., Shohag, M.H., Kozawa, K., Kato, K., Zhang, X., Yura, Y., Matsuura, Y., Kataoka, C., Nishioka, T., and Kaibuchi, K. 2015. Kinase-interacting substrate screening is a novel method to identify kinase substrates. *J. Cell Biol.*, **209**:895-912.
- Amano, M., Ito, M., Kimura, K., Fukata, Y., Chihara, K., Nakano, T., Matsuura, Y., and Kaibuchi, K. 1996. Phosphorylation and activation of myosin by Rho-associated kinase (Rho-kinase). *J. Biol. Chem.*, **271**:20246-20249.
- Amano, M., Nakayama, M., and Kaibuchi, K. 2010. Rho-kinase/ROCK: A key regulator of the cytoskeleton and cell polarity. *Cytoskeleton (Hoboken, N.J.)*, **67**:545-554.
- Aoki, K. and Matsuda, M. 2009. Visualization of small GTPase activity with fluorescence resonance energy transfer-based biosensors. *Nat Protoc.*, **4**:1623-1631.
- Aoki, K., Komatsu, N., Hirata, E., Kamioka, Y., and Matsuda, M. 2012. Stable expression of FRET biosensors: a new light in cancer research. *Cancer Sci.*, **103**:614-619.
- Arencibia, J.M., Pastor-Flores, D., Bauer, A.F., Schulze, J.O., Biondi, R.M. 2013. AGC protein kinases: from structural mechanism of regulation to allosteric drug development for the treatment of human diseases. *Biochim Biophys Acta*, **1834**:1302-1321.
- Azim, A.C., Barkalow, K., Chou, J., Hartwig, J.H. 2000. Activation of the small GTPases, rac and cdc42, after ligation of the platelet PAR-1 receptor. *Blood*, **95**:959-964.
- Boyartchuk, V.L., Ashby, M.N. and Rine, J. 1997. Dual roles for Ste24p in yeast a-factor maturation: NH<sub>2</sub>-terminal proteolysis and COOH-terminal CAAX processing. *Science*, **275**:1796-1800.
- Bustelo, X.R., Sauzeau, V., Berenjeno, I.M. 2007. GTP-binding proteins of the Rho/Rac family: regulation, effectors and functions in vivo. *Bioessays*, **29**:356-370.
- Casey, P.J. and Seabra, M.C. 1996. Protein prenyltransferases. *J. Biol. Chem.*, **271**: 5289-5292.
- Cechin, S. R., Dunkley, P. R., and Rodnight, R. 2005. Signal transduction mechanisms involved in the proliferation of C6 glioma cells induced by lysophosphatidic acid.

*Neurochem. Res.* **30**:603–611.

Chaudhuri, B., Hoermann, F., and Frommer, W. B. 2011. Dynamic imaging of glucose flux impedance using FRET sensors in wild-type Arabidopsis plants. *J. Exp. Bot.* **62**: 2411-2417.

Chen, G., Hou, Z., Gulbranson, D.R., and Thomson, J.A. 2010. Actin-myosin contractility is responsible for the reduced viability of dissociated human embryonic stem cells. *Cell Stem Cell*, **7**:240-248.

Chevrier, V., Piel, M., Collomb, N., Saoudi, Y., Frank, R., Paintrand, M., Narumiya, S., Bornens, M., and Job, D. 2002. The Rho-associated protein kinase p160ROCK is required for centrosome positioning. *J Cell Biol*, **157**:807-817.

Choi, S.Y., Huang, P., Jenkins, G.M., Chan, D.C., Schiller, J., and Frohman, M.A. 2006. A common lipid links Mfn-mediated mitochondrial fusion and SNARE-regulated exocytosis. *Nat. Cell Biol*, **8**: 1255–1262.

Chong, C., Tan, L., Lim, L., and Manser, E. 2001. The mechanism of PAK activation: autophosphorylation events in both regulatory and kinase domains control activity. *J Biol Chem.*, **276**:17347-17353.

Clarke, S. 1992. Protein isoprenylation and methylation at carboxyl-terminal cysteine residues. *Annu. Rev. Biochem.*, **61**: 355–386.

Clarke, S., Vogel, J.P., Deschenes, R.J. and Stock, J.B. 1988. Posttranslational modification of the Ha-ras oncogene protein: evidence for a third class of protein carboxyl methyltransferases. *Proc. Natl. Acad. Sci. U.S.A.*, **85**: 4643–4647.

Coleman, M.L. and Olson, M.F. 2002. Rho GTPase signalling pathways in the morphological changes associated with apoptosis. *Cell Death Differ.*, **9**:493-504.

Coleman, M.L., Sahai, E.A., Yeo, M., Bosch, M., Dewar, A., and Olson, M.F. 2001. Membrane blebbing during apoptosis results from caspase-mediated activation of ROCK I. *Nat Cell Biol.*, **3**:339-345.

Croft, D.R., and Olson, M.F. 2006. The Rho GTPase effector ROCK regulates cyclin A, cyclin D1, and p27Kip1 levels by distinct mechanisms. *Mol Cell Biol.* **26**:4612-4627.

De, A., Loening, A.M., and Gambhir, S.S. 2007. An improved bioluminescence resonance energy transfer strategy for imaging intracellular events in single cells and living subjects. *Cancer Res.* **67**:7175–7183.

De, A., Ray, P., Loening, A.M., and Gambhir, S.S. 2009. BRET: a red-shifted

bioluminescence resonance energy transfer (BRET)-based integrated platform for imaging protein-protein interactions from single live cells and living animals. *FASEB J.* **23**:2702–2709.

Dingwall, C., and Laskey, R. A. 1991. Nuclear targeting sequences--a consensus? *Trends Biochem. Sci.* **16**:478-481.

Dragulescu-Andrasi, A., Chan, C.T., De, A., Massoud, T.F., and Gambhir, S.S. 2011. Bioluminescence resonance energy transfer (BRET) imaging of protein-protein interactions within deep tissues of living subjects. *Proc Natl Acad Sci USA*, **108**:12060–12065.

Etienne-Manneville, S. and Hall, A. 2002. Rho GTPases in cell biology. *Nature (London)*, **420**:629-635.

Feng, J., Ito, M., Ichikawa, K., Isaka, N., Nishikawa, M., Hart-shorne, D.J. and Nakano, T. 1999. Inhibitory phosphorylation site for Rho-associated kinase on smooth muscle myosin phosphatase. *J. Biol. Chem.* **274**: 37385-37390.

Fischer, U., Huber, J., Boelens, W.C., Mattaj, I.W., and Lührmann, R. 1995. The HIV-1 Rev activation domain is a nuclear export signal that accesses an export pathway used by specific cellular RNAs. *Cell*, **82**: 475–483.

Fukata, M., Nakagawa, M., and Kaibuchi, K. 2003. Roles of Rho-family GTPases in cell polarisation and directional migration. *Curr. Opin. Cell Biol.*, **15**:590-597.

Gerard, R.D. and Gluzman, Y.1985. New host cell system for regulated simian virus 40 DNA replication. *Mol. Cell. Biol.*, **5**: 3231-3240.

Gluzman, Y. 1981. SV40-transformed simian cells support the replication of early SV40 mutant. *Cell*, **23**: 175-182.

Glyn, M.C., Lawrenson, J.G., and Ward, B.J. 2003. A Rho-associated kinase mitigates reperfusion-induced change in the shape of cardiac capillary endothelial cells in situ. *Cardiovasc Res*, **57**:195-206;

Goedhart, J., van Weeren, L., Hink, M.A., Vischer, N.O., Jalink, K., and Gadella, T.W., Jr. 2010. Bright cyan fluorescent protein variants identified by fluorescence lifetime screening. *Nat. Methods*, **7**: 137–139.

Gorlich, D., Prehn, S., Laskey, R. A., and Hartmann, E. 1994. Isolation of a protein that is essential for the first step of nuclear protein import. *Cell*, **79**: 767–778.

Goto, H., Kosako, H., Tanabe, K., Yanagida, M., Sakurai, M., Amano, M., Kaibuchi, K., and Inagaki, M. 1998. Phosphorylation of vimentin by Rho-associated kinase at a

unique amino-terminal site that is specifically phosphorylated during cytokinesis. *J. Biol. Chem.*, **273**:11728-11736.

Hall, A. 1998. Rho GTPases and the actin cytoskeleton. *Science*, **279**: 509–514.

Hamdan, F.F., Audet, M., Garneau, P., Pelletier, J., and Bouvier, M. 2005. High-throughput screening of G protein-coupled receptor antagonists using a bioluminescence resonance energy transfer 1-based  $\beta$ -arrestin2 recruitment assay. *J. Biomol Screen*, **10**:463–475.

Harada, A., Katoh, H., and Negishi, M. 2005. Direct interaction of Rnd1 with FRS2 beta regulates Rnd1-induced down-regulation of RhoA activity and is involved in fibroblast growth factor-induced neurite outgrowth in PC12 cells. *J. Biol. Chem.*, **280**:18418–18424.

Harvey, S. A., Anderson, S. C., and SundarRaj N. 2004. Downstream effects of ROCK signaling in cultured human corneal stromal cells: microarray analysis of gene expression. *Investig. Ophthalmol. Vis. Sci.* **45**:2168–2176.

He, H., Pannequin, J., Tantiogco, J. P., Shulkes, A. and Baldwin, G. S. 2005. Glycine-extended gastrin stimulates cell proliferation and migration through a Rho- and ROCK-dependent pathway, not a Rac/Cdc42-dependent pathway. *Am. J. Physiol. Gastrointest. Liver Physiol.* **289**:G478–G488.

Herzberg, R.P. 2009. Design and implementation of high-throughput screening assay. *Methods Mol Biol.*, **565**:1–32.

Hires, S.A., Zhu, Y., and Tsien, R.Y. 2008. Optical measurement of synaptic glutamate spillover and reuptake by linker optimized glutamate-sensitive fluorescent reporters. *Proc. Natl. Acad. Sci. USA*, **105**: 4411–4416.

Iizuka, M., Kimura, K., Wang, S., Kato, K., Amano, M., Kaibuchi, K., and Mizoguchi, A. 2012. Distinct distribution and localization of Rho-kinase in mouse epithelial, muscle and neural tissues. *Cell Struct. Funct.*, **37**:155-175.

Imamura, H., Nhat, K.P., Togawa, H., Saito, K., Iino, R., Kato-Yamada, Y., Nagai, T., and Noji, H. 2009. Visualization of ATP levels inside single living cells with fluorescence resonance energy transfer-based genetically encoded indicators. *Proc. Natl. Acad. Sci. USA*, **106**: 15651–15656.

Inada, H., Togashi, H., Nakamura, Y., Kaibuchi, K., Nagata, K., and Inagaki, M. 1999. Balance between activities of Rho kinase and type 1 protein phosphatase modulates turnover of phosphorylation and dynamics of desmin/ vimentin filaments. *J Biol Chem*,

**274:** 34932- 34939.

Ishizaki, T., Maekawa, M., Fujisawa, K., Okawa, K., Iwamatsu, A., Fujita, A., Watanabe, N., Saito, Y., Kakizuka, A., Morii, N., and Narumiya, S. 1996. The small GTP-binding protein Rho binds to and activates a 160 kDa Ser/Thr protein kinase homologous to myotonic dystrophy kinase. *EMBO J.*, **15**:1885-1893.

Iwamoto, H., M. Nakamura, S. Tada, R. Sugimoto, M. Enjoji, and H. Nawata. 2000. A p160ROCK-specific inhibitor, Y-27632, attenuates rat hepatic stellate cell growth. *J. Hepatol.* **32**:762–770.

Jensen, J.B., Lyssand, J.S., Hague, C., and Hille, B. 2009. Fluorescence changes reveal kinetic steps of muscarinic receptor-mediated modulation of phosphoinositides and Kv7.2/7.3 K<sup>+</sup> channels. *J Gen Physiol*, **133**:347–359.

Johnsson, A.K., Dai, Y., Nobis, M., Baker, M.J., McGhee, E.J., Walker, S., Schwarz, J.P., Kadir, S., Morton, J.P., Myant, K.B., Huels, D.J., Segonds-Pichon, A., Sansom, O.J., Anderson, K.I., Timpson, P., and Welch, H.C. 2014. The Rac-FRET mouse reveals tight spatiotemporal control of Rac activity in primary cells and tissues. *Cell Reports*, **6**:1153-1164.

Julian, L. and Olson, M.F. 2014. Rho-associated coiled-coil containing kinases (ROCK): structure, regulation, and functions. *Small GTPases*, **5**:e29846.

Kalderon, D., Richardson, W.D., Markham, A.F., Smith, A.E. 1984. Sequence requirements for nuclear location of simian virus 40 large-T antigen. *Nature*, **311**: 33–38.

Kamioka, Y., Sumiyama, K., Mizuno, R., Sakai, Y., Hirata, E., Kiyokawa, E., and Matsuda, M. 2012. Live imaging of protein kinase activities in transgenic mice expressing FRET biosensors. *Cell Struct. Funct.*, **37**:65-73.

Katoh, K., Kano, Y., Amano, M., Onishi, H., Kaibuchi, K., Fujiwara, K. 2001. Rho-kinase--mediated contraction of isolated stress fibers. *J Cell Biol*, **153**:569- 584;

Kawabata, S., Usukura, J., Morone, N., Ito, M., Iwamatsu, A., Kaibuchi, K., and Amano, M. 2004. Interaction of Rho- kinase with myosin II at stress fibres. *Genes Cells*, **9**:653-660.

Kimura, K., Ito, M., Amano, M., Chihara, K., Fukata, Y., Nakafuku, M., Yxamamori, B., Feng, J.H., Nakano, T., Okawa, K., Iwamatsu, A., and Kaibuchi, K. 1996. Regulation of myosin phosphatase by Rho and Rho-Associated kinase (Rho-kinase). *Science*, **273**:245-248.

- Knaus, U.G., Morris, S., Dong, H.J., Chernoff, J., and Bokoch, G.M. 1995. Regulation of human leucocyte p21- activated kinases through G protein-coupled receptors. *Science*, **269**:221-223.
- Knaus, U.G., Wang, Y., Reilly, A.M., Warnock, D., and Jackson, J.H. 1998. Structural requirements for PAK activation by Rac GTPases. *J Biol Chem.*, **273**: 21512-21518.
- Komatsu, N., Aoki, K., Yamada, M., Yukinaga, H., Fujita, Y., Kamioka, Y., and Matsuda, M. 2011. Development of an optimized backbone of FRET biosensors for kinases and GTPases. *Mol. Biol. Cell.*, **22**:4647-4656.
- Kosako, H., Amano, M., Yanagida, M., Tanabe, K., Nishi, Y., Kaibuchi, K., and Inagaki, M. 1997. Phosphorylation of glial fibrillary acidic protein at the same sites by cleavage furrow kinase and Rho-associated kinase. *J. Biol. Chem.*, **272**:10333-10336.
- Kosako, H., Yoshida, T., Matsumura, F., Ishizaki, T., Narumiya, S., and Inagaki, M. 2000. Rho-kinase/ROCK is involved in cytokinesis through the phosphorylation of myosin light chain and not ezrin/radixin/moesin proteins at the cleavage furrow. *Oncogene*, **19**:6059-6064.
- Kosako, H., Goto, H., Yanagida, M., Matsuzawa, K., Fujita, M., Tomono, Y., Okigaki, T., Odai, H., Kaibuchi, K., and Inagaki, M. 1999. Specific accumulation of Rho-associated kinase at the cleavage furrow during cytokinesis: cleavage furrow-specific phosphorylation of intermediate filaments. *Oncogene*, **18**:2783- 2788.
- Kümper, S., Mardakheh, F.K., McCarthy, A., Yeo, M., Stamp, G.W., Paul, A., Worboys, J., Sadok, A., Jorgensen, C., Guichard, S., and Marshall, C.J. 2016. Rho-associated kinase (ROCK) function is essential for cell cycle progression, senescence and tumorigenesis. *Elife*. **5**:e12994.
- Lanford, R.E., and Butel, J.S. 1984. Construction and characterization of an SV40 mutant defective in nuclear transport of T antigen. *Cell*, **37**: 801–813.
- Leung, T., Chen, X.Q., Manser, E. and Lim, L. 1996. The p160 RhoA-binding kinase ROK alpha is a member of a kinase family and is involved in the reorganization of the cytoskeleton. *Mol. Cell. Biol.* **16**: 5313-5327.
- Leung, T., Manser, E., Tan, L., and Lim, L. 1995. A novel serine/ threonine kinase binding the Ras-related RhoA GTPase which translocates the kinase to peripheral membranes. *J Biol Chem*, **270**:29051- 29054.
- Loening, A.M., Fenn, T.D., Wu, A.M., and Gambhir, S.S. 2006. Consensus guided mutagenesis of Renilla luciferase yields enhanced stability and light output. *Protein Eng*

*Des Sel*, **19**:391–400.

Lohse, M.J., Nikolaev, V.O., Hein, P., Hoffmann, C., Vilardaga, J.P., and Bünemann, M. 2008. Optical techniques to analyze real-time activation and signaling of G-protein-coupled receptors. *Trends Pharmacol Sci*, **29**:159–165.

Ma, Z., Kanai, M., Kawamura, K., Kaibuchi, K., Ye, K., and Fukasawa, K. 2006. Interaction between ROCK II and nucleophosmin/B23 in the regulation of centrosome duplication. *Mol Cell Biol*, **26**:9016-9034.

Manser, E., Leung, T., Salihuddin, H., Zhao, Z.S, and Lim, L. 1994. A brain serine/threonine protein kinase activated by Cdc42 and Rac1. *Nature*. **367**:40- 46.

Matsui, T., Amano, M., Yamamoto, T., Chihara, K., Nakafuku, M., Ito, M., Nakano, T., Okawa, K., Iwamatsu, A., and Kaibuchi, K. 1996. Rho-associated kinase, a novel serine/ threonine kinase, as a putative target for small GTP binding protein Rho. *EMBO J.*, **15**:2208-2216.

Miura, H., Matsuda, M., and Aoki, K. 2014. Development of a FRET biosensor with high specificity for Akt. *Cell Struct. Funct.*, **39**:9-20.

Miyawaki, A. and Niino, Y. 2015. Molecular spies for bioimaging--fluorescent protein-based probes. *Mol. Cell.*, **58**:632-643.

Mori, K., Amano, M., Takefuji, M., Kato, K., Morita, Y., Nishioka, T., Matsuura, Y., Murohara, T., and Kaibuchi, K. 2009. Rho-kinase contributes to sustained RhoA activation through phosphorylation of p190A RhoGAP. *J. Biol. Chem.*, **284**:5067-5076.

Nagai, T., Yamada, S., Tominaga, T., Ichikawa, M., and Miyawaki, A. 2004. Expanded dynamic range of fluorescent indicators for Ca(2+) by circularly permuted yellow fluorescent proteins. *Proc. Natl. Acad. Sci. USA*, **101**: 10554–10559.

Nakagawa, O., Fujisawa, K., Ishizaki, T., Saito, Y., Nakao, K., and Narumiya, S. 1996. ROCK-I and ROCK-II, two isoforms of Rho-associated coiled-coil forming protein serine/threonine kinase in mice. *FEBS Lett.*, **392**:189-193.

Narumiya, S., Tanji, M., and Ishizaki, T. 2009. Rho signaling, ROCK and mDia1, in transformation, metastasis and invasion. *Cancer Metastasis Rev.*, **28**:65-76.

Nishimaki, H., Kasai, K., Kozaki, K., Takeo, T., Ikeda, H., Saga, S., Nitta, M., and Itoh, G. 2004. A role of activated Sonic hedgehog signaling for the cellular proliferation of oral squamous cell carcinoma cell line. *Biochem. Biophys. Res. Commun.* **314**:313–320.

Niwa, H., Yamamura, K., and Miyazaki, J. 1991. Efficient selection for high-expression transfectants with a novel eukaryotic vector. *Gene*, **108**:193-200.

- Nobes, C.D., and Hall, A. 1995. Rho, Rac and Cdc42 GTPases regulate the assembly of multimolecular focal complexes associated with actin stress fibers, lamellipodia and filopodia. *Cell*, **81**:53-62.
- Ohgushi, M. and Sasai, Y. 2011. Lonely death dance of human pluripotent stem cells: ROCKing between metastable cell states. *Trends Cell Biol.*, **21**:274-282.
- Ohgushi, M., Matsumura, M., Eiraku, M., Murakami, K., Aramaki, T., Nishiyama, A., Muguruma, K., Nakano, T., Suga, H., Ueno, M., Ishizaki, T., Suemori, H., Narumiya, S., Niwa, H., and Sasai, Y. 2010. Molecular pathway and cell state responsible for dissociation-induced apoptosis in human pluripotent stem cells. *Cell Stem Cell*, **7**:225-239.
- Oldach, L. and Zhang, J. 2014. Genetically encoded fluorescent biosensors for live-cell visualization of protein phosphorylation. *Chem. Biol.*, **21**:186-197.
- Otto, J.C., Kim, E., Young, S.G. and Casey, P.J. 1999. Cloning and characterization of a mammalian prenyl protein-specific protease. *J. Biol. Chem.*, **274**: 8379–8382.
- Pearce, L.R., Komander, D., and Alessi, D.R. 2010. The nuts and bolts of AGC protein kinases. *Nat Rev Mol Cell Biol.*, **11**:9-22.
- Pelosi, M., Marampon, F., Zani, B.M., Prudente, S., Perlas, E., Caputo, V., Cianetti, L., Berno, V., Narumiya, S., and Kang, S.W. 2007. ROCK2 and its alternatively spliced isoform ROCK2m positively control the maturation of the myogenic program. *Mol Cell Biol*, **27**:6163-6176.
- Porter, K. E., N. A. Turner, D. J. O'Regan, A. J. Balmforth, and S. G. Ball. 2004. Simvastatin reduces human atrial myofibroblast proliferation independently of cholesterol lowering via inhibition of RhoA. *Cardiovasc. Res.* **61**:745–755.
- Prasher, D.C., Eckenrode, V.K., and Ward, W.W.; Prendergast, F.G.; Cormier, M.J. 1992. Primary structure of the *Aequorea victoria* green-fluorescent protein. *Gene*, **111**: 229–233.
- Potzkei, J., Kunze, M., Drepper, T., Gensch, T., Jaeger, K.E., and Buchs, J. 2012. Real-time determination of intracellular oxygen in bacteria using a genetically encoded FRET-based biosensor. *BMC Biol.*, **10**: 28.
- Prior, I.A., Harding, A., Yan, J., Sluimer, J., Parton, R.G., and Hancock, J.F. 2001. GTP-dependent segregation of H-ras from lipid rafts is required for biological activity. *Nat. Cell Biol*, **3**: 368–375.
- Radu, A., Blobel, G., and Moore, M. S. 1995. Identification of a protein complex that is

required for nuclear protein import and mediates docking of import substrate to distinct nucleoporins. *Proc. Natl. Acad. Sci. U. S. A.* **92**:1769–1773.

Rees, R. W., N. A. Foxwell, D. J. Ralph, P. D. Kell, S. Moncada, and S. Celtek. 2003. Y-27632, a Rho-kinase inhibitor, inhibits proliferation and adrenergic contraction of prostatic smooth muscle cells. *J. Urol.* **170**:2517–2522.

Ridley, A., Paterson, H.F., Johnston, C., Diekmann, D., and Hall, A. 1992. The small GTP-binding protein rac regulates growth factor-induced membrane ruffling. *Cell*, **70**:401-410.

Riento, K. and Ridley, A.J. 2003. Rocks: multifunctional kinases in cell behaviour. *Nature reviews. Molecular Cell Biology*, **4**:446-456.

Rizzo, M.A., Springer, G.H., Granada, B., and Piston, D.W. 2004. An improved cyan fluorescent protein variant useful for FRET. *Nat. Biotechnol.*, **22**: 445–449.

Robbins, J., Dilworth, S. M., Laskey, R. A., and Dingwall, C. 1991. Two interdependent basic domains in nucleoplasmin nuclear targeting sequence: identification of a class of bipartite nuclear targeting sequence. *Cell*, **64**: 615–623.

Robinson, K.H., Yang, J.R, and Zhang, J. 2014. FRET and BRET-Based Biosensors in Live Cell Compound Screens. *Methods Mol Biol.*, **1071**:217-225.

Rocks, O., Peyker, A., Kahms, M., Verveer, P.J., Koerner, C., Lumbierres, M., Kuhlmann, J., Waldmann, H., Wittinghofer, A., and Bastiaens, P.I. 2005. An acylation cycle regulates localization and activity of palmitoylated Ras isoforms. *Science*, **307**: 1746–1752.

Sample, V., Mehta, S., and Zhang, J. 2014. Genetically encoded molecular probes to visualize and perturb signaling dynamics in living biological systems. *J. Cell Sci.*, **127**:1151-1160.

Saito, K., Chang, Y.F., Horikawa, K., Hatsugai, N., Higuchi, Y., Hashida, M., Yoshida, Y., Matsuda, T., Arai, Y., and Nagai, T. 2012. Luminescent proteins for high-speed single-cell and whole-body imaging. *Nat. Commun.*, **3**: 1262–1270.

Schmandke, A., Schmandke, A., and Strittmatter, S.M. 2007. ROCK and Rho: biochemistry and neuronal functions of Rho-associated protein kinases. *The Neuroscientist : a review journal bringing neurobiology, neurology and psychiatry*, **13**:454-469.

Schwayer, C., Sikora, M., Slovakova, J., Kardos, R., and Heisenberg, C.P. 2016. Actin Rings of Power. *Dev Cell.*, **37**:493-506.

- Seasholtz, T. M., M. Majumdar, D. D. Kaplan, and J. H. Brown. 1999. Rho and Rho kinase mediate thrombin-stimulated vascular smooth muscle cell DNA synthesis and migration. *Circ. Res.* **84**:1186–1193.
- Sebbagh, M., Hamelin, J., Bertoglio, J., Solary, E., and Breard, J. 2005. Direct cleavage of ROCK II by granzyme B induces target cell membrane blebbing in a caspase-independent manner. *J. Exp. Med.*, **201**:465-471.
- Sebbagh, M., Renvoize, C., Hamelin, J., Riche, N., Bertoglio, J., and Breard, J. 2001. Caspase-3-mediated cleavage of ROCK I induces MLC phosphorylation and apoptotic membrane blebbing. *Nat Cell Biol.*, **3**:346-352.
- Seibold, S., D. Schurle, A. Heinloth, G. Wolf, M. Wagner, and J. Galle. 2004. Oxidized LDL induces proliferation and hypertrophy in human umbilical vein endothelial cells via regulation of p27Kip1 expression: role of RhoA. *J. Am. Soc. Nephrol.* **15**:3026–3034.
- Sin, W.C., Chen, X.Q., Leung, T., Lim, L. 1998. RhoA-binding kinase alpha translocation is facilitated by the collapse of the vimentin intermediate filament network. *Mol Cell Biol*, **18**:6325-6339.
- Sorensen, S. D., O. Nicole, R. D. Peavy, L. M. Montoya, C. J. Lee, T. J. Murphy, S. F. Traynelis, and J. R. Hepler. 2003. Common signaling pathways link activation of murine PAR-1, LPA, and S1P receptors to proliferation of astrocytes. *Mol. Pharmacol.* **64**:1199–1209.
- Stade, K., Ford, C. S., Guthrie, C., and Weis, K. 1997. Exportin 1 (Crm1p) is an essential nuclear export factor. *Cell*, **90**: 1041–1050.
- Stroeken, P.J., Alvarez, B., Van Rheenen, J., Wijnands, Y.M., Geerts, D., Jalink, K., and Roos, E. 2006. Integrin cytoplasmic domain-associated protein-1 (ICAP-1) interacts with the ROCK-I kinase at the plasma membrane. *J Cell Physiol*, **208**:620-628.
- Suh, B.C., Inoue, T., Meyer, T., and Hille, B. 2006. Rapid chemically induced changes of PtdIns(4,5)P2 gate KCNQ ion channels. *Science*, **314**:1454-1457.
- Tanaka, T., Nishimura, D., Wu, R.C., Amano, M., Iso, T., Kedes, L., Nishida, H., Kaibuchi, K., and Hamamori, Y. 2006. Nuclear Rho kinase, ROCK2, targets p300 acetyltransferase. *J Biol Chem*, **281**:15320-15329.
- Tharoux, P. L., R. C. Bukoski, P. N. Rocha, S. D. Crowley, P. Ruiz, C. Nataraj, D. N. Howell, K. Kaibuchi, R. F. Spurney, and T. M. Coffman. 2003. Rho kinase promotes alloimmune responses by regulating the proliferation and structure of T cells. *J.*

*Immunol.* **171**:96–105.

Thumkeo, D., Watanabe, S., and Narumiya, S. 2013. Physiological roles of Rho and Rho effectors in mammals. *Eur. J. Cell Biol.*, **92**:303-315.

Tominaga, T., Sahai, E., Chardin, P., McCormick, F., Courtneidge, S.A., and Alberts, A.S. 2000. Diaphanous-related formins bridge Rho GTPase and Src tyrosine kinase signaling. *Mol. Cell*, **5**: 13–25.

Tran Quang, C., Gautreau, A., Arpin, M., and Treisman, R. 2000. Ezrin function is required for ROCK-mediated fibroblast transformation by the Net and Dbl oncogenes. *EMBO J.*, **19**:4565-4576.

Uehata, M., Ishizaki, T., Satoh, H., Ono, T., Kawahara, T., Morishita, T., Tamakawa, H., Yamagami, K., Inui, J., Maekawa, M., and Narumiya, S. 1997. Calcium sensitization of smooth muscle mediated by a Rho-associated protein kinase in hypertension. *Nature*, **389**:990-994.

Urrea, J., Sandoval, M., Cornejo, I., Barros, L.F., Sepulveda, F.V., and Cid, L.P. 2008. A genetically encoded ratiometric sensor to measure extracellular pH in microdomains bounded by basolateral membranes of epithelial cells. *Pflugers Arch.*, **457**: 233–242.

Valencia, A., Chardin, P., Wittinghofer, A. and Sander, C. 1991. The Ras protein family: evolutionary tree and role of conserved amino acids. *Biochemistry*, **30**: 4637-4648.

Van Aelst, L., and D'Souza-Schorey, C. 1997. Rho GTPases and signaling networks. *Genes Dev.* **11**: 2295–2322.

Van der Krogt, G.N., Ogink, J., Ponsioen, B., and Jalink, K. 2008. A comparison of donor-acceptor pairs for genetically encoded FRET sensors: Application to the Epac cAMP sensor as an example. *PLoS ONE*, **3**: e1916.

Van Unen, J., Reinhard, N.R., Yin, T., Wu, Y.I., Postma, M., Gadella, T.W., and Goedhart, J. 2015. Plasma membrane restricted RhoGEF activity is sufficient for RhoA-mediated actin polymerization. *Sci Rep*, **5**:14693.

Vandenabeele, P., Galluzzi, L., Vanden Berghe, T., and Kroemer, G. 2010. Molecular mechanisms of necroptosis: an ordered cellular explosion. *Nat Rev Mol Cell Biol*, **11**:700-714.

Vega, F.M., Fruhwirth, G., Ng, T., and Ridley, A.J. 2011. RhoA and RhoC have distinct roles in migration and invasion by acting through different targets. *J. Cell Biol.* **193**:655-665.

Vichalkovski, A., K. Baltensperger, D. Thomann, and H. Porzig. 2005. Two different

pathways link G-protein-coupled receptors with tyrosine kinases for the modulation of growth and survival in human hematopoietic progenitor cells. *Cell Signal*. **17**:447–459.

Walker, A., Su, H., Conti, M.A., Harb, N., Adelstein, R.S., and Sato, N. 2010. Non-muscle myosin II regulates survival threshold of pluripotent stem cells. *Nat Commun*, **1**:71.

Wang, G., A. Woods, S. Sabari, L. Pagnotta, L. A. Stanton, and F. Beier. 2004. RhoA/ROCK signaling suppresses hypertrophic chondrocyte differentiation. *J. Biol. Chem.* **279**:13205–13214.

Watanabe, K., Ueno, M., Kamiya, D., Nishiyama, A., Matsumura, M., Wataya, T., Takahashi, J.B., Nishikawa, S., Muguruma, K., and Sasai, Y. 2007. A ROCK inhibitor permits survival of dissociated human embryonic stem cells. *Nat. Biotechnol.*, **25**:681-686.

Watanabe, N., Kato, T., Fujita, A., Ishizaki, T., and Narumiya, S. 1999. Cooperation between mDia1 and ROCK in Rho-induced actin reorganization. *Nature Cell Biol.* **1**: 136–143.

Wen, W., Meinkoth, J.L., Tsien, R.Y., and Taylor, S.S. 1995. Identification of a signal for rapid export of proteins from the nucleus. *Cell*, **82**: 463–473.

Wennerberg, K., and Der, C.J. 2004. Rho-family GTPases: it's not only Rac and Rho (and I like it). *J Cell Sci.*, **117**: 1301-1312.

Wennerberg, K., Forget, M. A., Ellerbroek, S. M., Arthur, W. T., BurrIDGE, K., Settleman, J., Der, C. J., and Hansen, S. H. 2003. Rnd proteins function as RhoA antagonists by activating p190 RhoGAP. *Curr. Biol.* **13**, 1106 –1115.

Wheeler, A. P., and Ridley, A. J. 2004. Why three Rho proteins? RhoA, RhoB, RhoC, and cell motility. *Exp. Cell Res.*, **301**: 43–49.

Winter-Vann, A.M., and Casey, P.J. 2005. Post-prenylation-processing enzymes as new targets in oncogenesis. *Nat Rev Cancer*, **5**:405–412.

Wooldridge, A.A., MacDonald, J.A., Erdodi, F., Ma, C., Borman, M.A., Hartshorne, D.J., and Haystead, T.A. 2004. Smooth muscle phosphatase is regulated in vivo by exclusion of phosphorylation of threonine 696 of MYPT1 by phosphorylation of Serine 695 in response to cyclic nucleotides. *J. Biol. Chem.*, **279**:34496-34504.

Xia, Z., and Rao, J. 2009. Biosensing and imaging based on bioluminescence resonance energy transfer. *Curr. Opin. Biotechnol.*, **20**: 37–44.

Xu, X., Brzostowski, J.A., and Jin, T. 2009. Monitoring dynamic GPCR signaling

events using fluorescence microscopy, FRET imaging, and single-molecule imaging. *Methods Mol Biol*, **571**:371–383.

Yoshizaki, H., Ohba, Y., Kurokawa, K., Itoh, R.E., Nakamura, T., Mochizuki, N., Nagashima, K., and Matsuda, M. 2003. Activity of Rho-family GTPases during cell division as visualized with FRET-based probes. *J. Cell Biol.*, **162**:223-232.

Yoshizaki, H., Ohba, Y., Parrini, M.C., Dulyaninova, N.G., Bresnick, A.R., Mochizuki, N., and Matsuda, M. 2004. Cell type-specific regulation of RhoA activity during cytokinesis. *J. Biol. Chem.*, **279**:44759-44762.

Yusa, K., Rad, R., Takeda, J., and Bradley, A. 2009. Generation of transgene-free induced pluripotent mouse stem cells by the piggyBac transposon. *Nat Methods*, **6**:363-369.

Zacharias, D.A., Violin, J.D., Newton, A.C., and Tsien, R.Y. 2002. Partitioning of lipid-modified monomeric GFPs into membrane micro-domains of live cells. *Science*, **296**: 913–916.

Zenke, F.T., King, C.C., Bohl, B.P., and Bokoch, G.M. 1999. Identification of a central phosphorylation site in p21- activated kinase regulating autoinhibition and kinase activity. *J Biol Chem.*, **274**:32565-32573.

Zhang, J., Ma, Y., Taylor, S.S., and Tsien, R.Y. 2001. Genetically encoded reporters of protein kinase activity reveal impact of substrate tethering. *Proc. Natl. Acad. Sci. U.S.A.*, **98**:14997-15002.

Zhao, Z., and Rivkees, S. A. 2003. Rho-associated kinases play an essential role in cardiac morphogenesis and cardiomyocyte proliferation. *Dev. Dyn.* **226**:24–32.

Zhong, S., Navaratnam, D., and Santos-Sacchi, J. 2014. A genetically-encoded YFP sensor with enhanced chloride sensitivity, photostability and reduced pH interference demonstrates augmented transmembrane chloride movement by Gerbil Prestin (SLC26a5). *PLOS ONE*, **9**: e99095.

## **Acknowledgment**

The thesis would not be completed without the support of many people.

My supervisor, Professor Michiyuki Matsuda, has been a significant presence during my doctorate course. His critical comments and suggestions on each part of the research have strengthened this study significantly. I will always be thankful for his persistent guidance and encouragement.

I am grateful to Dr. Kazuhiro Aoki, Dr. Kenta Terai, Dr. Naoki Komatsu, and Dr. Masamichi Imajo, for keeping their hearts whenever I want a talk. Their wisdom, knowledge and professional experience has been beneficial to this study in many aspects. I wish to thank them for their countless hours of reflecting, reading, encouraging, and most of all patience throughout the entire process.

In addition, I want to thank Ms. Akiko Kawagishi, Ms. Hirano Kyouto, Ms. Naoko Nishimoto, Ms. Naoko Koizumi, Ms. Kobayashi Sachiko and Mrs. Kanako Takakura for their technical support during my Ph.D. course.

Thanks to my numerous colleagues, Noriyuki Kawabata, Take Sano, Yuzhe Li, Akira Komatsubara, Masaru Muta, Haruko Miura, Yumi Konagaya, Gembu Maryu, Yoshinobu Konishi, Ayako Imanishi, Youichi Uda, and Tomoaki Kinjo, who endured this long process with me, always offering support and encouragement.

Finally, I would like to thank to China Scholarship Council for awarding me a generous scholarship, providing me with the financial means to complete this project.

This thesis is based on material contained in the following scholarly paper. Chunjie Li, Ayako Imanishi, Naoki Komatsu<sup>1</sup>, Kenta Terai, Mutsuki Amano, Kozo Kaibuchi, and Michiyuki Matsuda. A FRET biosensor for ROCK based on a consensus substrate sequence identified by KISS technology. *Cell Structure and Function*, in press, 2017.